AEDC-TR-10-T-6

Flight-Ready TDLAS Combustion Sensor for the HIFiRE 2 Hypersonic Research Program

Andrew D. Sappey, Ph.D.
Lee Sutherland
David Owenby
Paul VanHoudt
Jerry Hannam
Qingchun Zhoa, Ph.D.
Patrick J. McCormick
Bernard P. Masterson, Ph.D.
Michael Estes, Ph.D.

Zolo Technologies, Inc.

September 2009

Final Report for Period 1 October 2006 – 14 August 2009

**ARNOLD ENGINEERING DEVELOPMENT CENTER
ARNOLD AIR FORCE BASE, TENNESSEE
AIR FORCE MATERIEL COMMAND
UNITED STATES AIR FORCE**

NOTICES

When U. S. Government drawings, specifications, or other data are used for any purpose other than a definitely related Government procurement operation, the Government thereby incurs no responsibility nor any obligation whatsoever, and the fact that the Government may have formulated, furnished, or in any way supplied the said drawings, specifications, or other data, is not to be regarded by implication or otherwise, as in any manner licensing the holder or any other person or corporation, or conveying any rights or permission to manufacture, use, or sell any patented invention that may in any way be related thereto.

Qualified users may obtain copies of this report from the Defense Technical Information Center.

References to named commercial products in this report are not to be considered in any sense as an endorsement of the product by the United States Air Force or the Government.

DESTRUCTION NOTICE

For unclassified, limited documents, destroy by any method
that will prevent disclosure or reconstruction of the document.

APPROVAL STATEMENT

This report has been reviewed and approved.

STEVEN A. BANCROFT
T&E S&T APTT Focus Area Program Manager
AEDC/649th TESS/PI

Approved for publication:

FOR THE COMMANDER

THOMAS P. FETTERHOFF
Technical Director, Technology Division
AEDC/649th TESS/GCA

REPORT DOCUMENTATION PAGE		*Form Approved* *OMB No. 0704-0188*

The public reporting burden for this collection of information is estimated to average 1 hour per response, including the time for reviewing instructions, searching existing data sources, gathering and maintaining the data needed, and completing and reviewing the collection of information. Send comments regarding this burden estimate or any other aspect of this collection of information, including suggestions for reducing the burden, to Department of Defense, Washington Headquarters Services, Directorate for Information Operations and Reports (0704-0188), 1215 Jefferson Davis Highway, Suite 1204, Arlington, VA 22202-4302. Respondents should be aware that notwithstanding any other provision of law, no person shall be subject to any penalty for failing to comply with a collection of information if it does not display a currently valid OMB control number.
PLEASE DO NOT RETURN YOUR FORM TO THE ABOVE ADDRESS

1. REPORT DATE (DD-MM-YYYY)	2. REPORT TYPE	3. DATES COVERED *(From – To)*
00-09-2009	Final Report	1 Oct. 2006-14 Aug. 2009

4. TITLE AND SUBTITLE	5a. CONTRACT NUMBER
Flight-Ready TDLAS Combustion Sensor for the HIFiRE 2 Hypersonic Research Program	FA9101-05-C-006
	5b. GRANT NUMBER
Final Report	
T&E/S&T APTT Project	5c. PROGRAM ELEMENT NUMBER

6. AUTHOR(S)	5d. PROJECT NUMBER
A. Sappey, L. Sutherland, D. Owenby, P.VanHoudt, J. Hannam, Q. Zhao, P. McCormick, B. Masterson, M. Estes	
	5e. TASK NUMBER
	5f. WORK UNIT NUMBER

7. PERFORMING ORGANIZATION NAME(S) AND ADDRESS(ES)	8. PERFORMING ORGANIZATION REPORT NO.
Zolo Technologies, Inc. 4946 N 63rd St., Boulder, Colorado 80301	ZD-2231

9. SPONSORING/MONITORING AGENCY NAME(S) AND ADDRESS(ES)	10. SPONSOR/MONITOR'S ACRONYM(S)
Test Resource Management Center	
1225 South Clark Street, Suite 1200	11. SPONSOR/MONITOR'S REPORT NUMBER(S)
Arlington, VA 22202	

12. DISTRIBUTION/AVAILABILITY STATEMENT
Distribution A

13. SUPPLEMENTARY NOTES
Available in the Defense Technical Information Center (DTIC).

14. ABSTRACT
Advanced air-breathing engine development requires new combustion diagnostics. The new sensors must not intrude into the engine and the sensing components must endure the thermal and vibrational environment near a scramjet combustor. The sensor should also be suitable as a diagnostic in realistic scramjet test situations, including in flight in sounding-rocket test vehicles. The development of a laser sensor meeting these requirements for the HIFiRE 2 hypersonic research program is described in this report.

15. Subject Terms
TDLAS, molecular absorption spectroscopy, diagnostics, hypersonics, flight hardware

16. SECURITY CLASSIFICATION OF:			17. LIMITATION OF ABSTRACT	18. NUMBER OF PAGES	19A. NAME OF RESPONSIBLE PERSON
A. REPORT	B. ABSTRACT	C. THIS PAGE			Steven Bancroft
			SAR		19B. TELEPHONE NUMBER *(Include area code)*
Unclassified	Unclassified	Unclassified			931-454-6418

Standard Form 298 (Rev. 8/98)
Prescribed by ANSI Std. 739.18

PREFACE

CONTENTS

ILLUSTRATIONS

LIST OF SYMBOLS AND ACRONYMS

ADC	analog to digital converter
AEDC	Arnold Engineering Development Center
AFRL	Air Force Research Laboratories
A_i	absorption area (cm^{-1})
α_{tot}	total molecular absorption
BRD	balanced ratiometric detection
c	speed of light in vacuum = 2.998×10^8 m/s
c_2	= hc/k = 1.438 cm^{-1}/K
$\delta\alpha$	absorption measurement uncertainty
DFB	distributed feedback
DSP	digital signal processor
DSTO	Defence Science and Technology Organisation (Australia)
δT	temperature measurement uncertainty (K)
E"	molecular lower-state energy (cm-1)
f	signal frequency (Hz)
f_{comp}	fraction of measurement time collecting data
FET	field effect transistor
FPGA	field-programmable gate array
f_{spec}	fraction of measurement time on absorption line
FWHM	absorption line width (cm^{-1})
$g_j(\nu)$	molecular absorption line shape function
h	Planck constant = 6.626×10^{-34} Js
HIFiRE	Hypersonic International Flight Research and Experimentation
I_{bkg}	background light photocurrent
I_s	detected photocurrent
k	Boltzmann constant = 1.38×10^{-23} J/K
L	absorption path length (cm)
NASA	National Aeronautics and Space Administration
n_{det}	detector noise in A/$Hz^{1/2}$
nm	nanometer
n_{mult}	multiplicative noise ($Hz^{-1/2}$)
n_{shot}	shot noise ($Hz^{-1/2}$)
NSROC	NASA Sounding Rocket Operations Contract
n_{TOT}	total photocurrent noise density in A/$Hz^{1/2}$
P	pressure in atmospheres
P_L	laser power (W)
pm	picometer
Q(T)	molecular partition function
range	scanning range (1.5 x absorption peak separation in cm^{-1})
R_{det}	photodiode responsivity (A/W)
$S_j(T)$	molecular absorption line strength
t	averaging time (s)
T	absolute temperature in K
TDLAS	tunable diode laser absorption spectroscopy
t_{eff}	effective averaging time (s)
T_{gas}	light transmission through a gas medium
TIA	transimpedance amplifier
WMS	wavelength modulation spectroscopy
x	molecule species concentration (% of total molecules)

1.0 INTRODUCTION

Advanced air-breathing engine development requires new combustion diagnostics. Because of the challenges of maximizing thrust and minimizing drag in supersonic combustion engines, sensitive monitors of temperature distribution, gas flow fields and combustion reactant and product concentrations are needed to validate combustion models and refine engine designs.

The new sensors must not intrude into the engine and the sensing components must endure the thermal and vibrational environment near a scramjet combustor. The sensor should also be suitable as a diagnostic in realistic scramjet test situations, including in flight in sounding-rocket test vehicles. This places demands on sensor size, power consumption and ruggedness.

Sensor Targets:
complete
combustion
stoichiometry
shock train
structure

N2, H2O, CO2,...

N2, O2, Ar
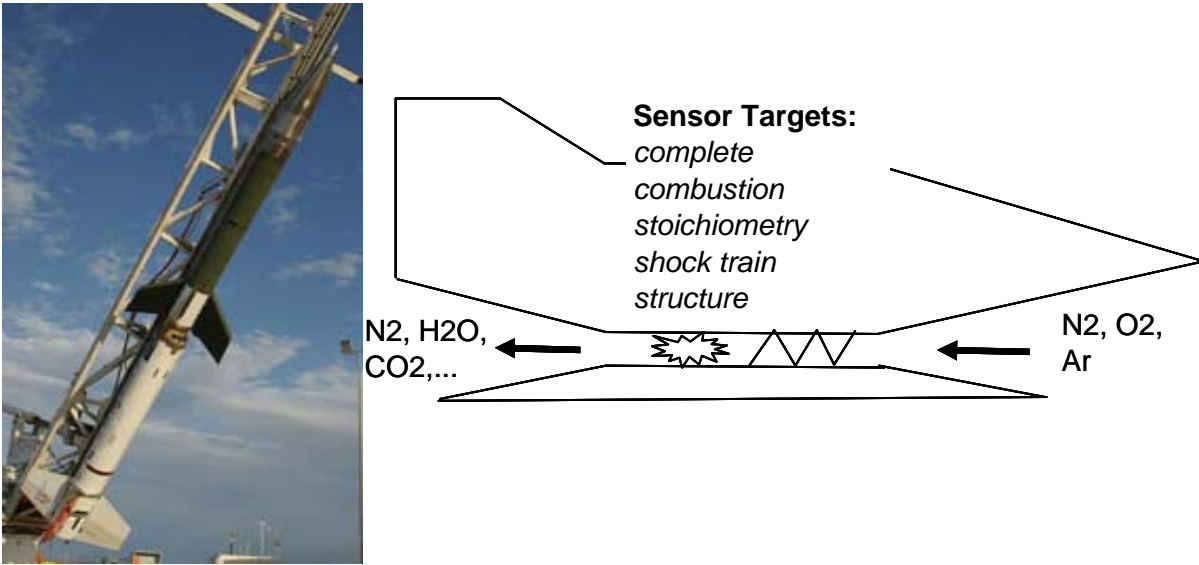
Figure 1a: HIFiRE Terrier-Orion sounding rocket
Figure 1b: hypersonic vehicle sensor targets

Zolo Technologies has collaborated with the Air Force Research Laboratory and Arnold Engineering Development Center to develop a sensor based on selective light absorption by water molecules to meet scramjet testing needs. The sensor was designed for flight in a sounding rocket as part of the Hypersonic International Flight Research and Experimentation (HIFiRE) program (1). The sensor is compact, rugged and has low power consumption. This report describes the sensor and its design.

2.0 MEASUREMENT PRINCIPLE

The Zolo sensor is based on Tunable Diode Laser Absorption Spectroscopy or TDLAS. This technique measures light absorption by target molecules at specific wavelengths in order to infer molecule concentration and temperature. In this case we sense water vapor, a combustion product with strong absorption lines in the 1300 - 1400 nm range accessible by high-performance telecommunications lasers. The High Temperature Gasdynamics Laboratory at Stanford University has pioneered the application of TDLAS to combustion and has developed techniques for measuring light absorption in harsh environments.(2)
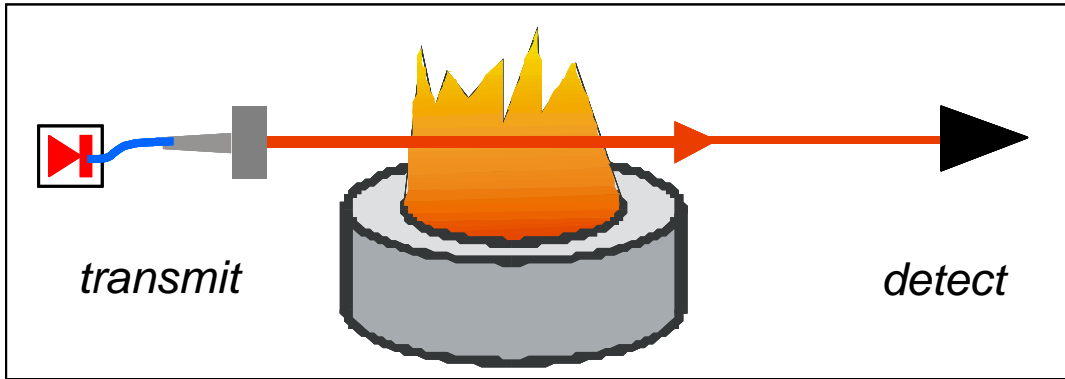
Figure 2: Tunable laser absorption spectroscopy experiment

When laser light passes through a gas sample as shown in Figure 2, specific wavelengths are absorbed which are a function of the absorbing molecule's temperature and pressure. The amount of absorption can be calculated from known physical constants and so knowing the amount of absorption allows one to infer properties such as gas temperature and density. The light absorption is described by Beer's Law:

$$T_{gas}(\nu) \; = \; exp[-\alpha_{tot}]$$

At a frequency ν near a set of absorption lines j, the total absorption is:

$$\alpha_{tot} = \int dz \; P(z) \; x(z) \; \Sigma \; S_j[T(z)] \; g_j[\nu-\nu_j, \; T(z), \; P(z)]$$

where

$P(z)$ = pressure in atm

$x(z)$ = target gas concentration

$T(z)$ = gas temperature in K

$S_j(T)$ = absorption line strength of the jth line in cm^{-2}/atm

$g_j(\nu)$ = normalized absorption line shape vs wavelength ($\int g(\nu) \, d\nu \; = \; 1$)

Assuming a uniform path, the absorption is:

$$\alpha_{tot} = P \; L \; x \; \Sigma \; S_j(T) \; g_j(\nu-\nu_j, \; T, \; P)$$

where L is the absorbing path length in centimeters.

For each absorption line j, the absorption line strength $S_j(T)$ depends on fundamental constants:

$$S_j(T) \; = \; S_{0j} \; [Q(T_0) \; T_0 \; / \; Q(T) \; T] \; exp[-c_2 \; E_j" \; (1/T - 1/T_0)]$$

where $Q(T)$ is the molecular partition function, T_0 is a reference temperature (conventionally, 296 K) at which the line strength is S_{0j} and $c_2 = hc/k$ is $1.438 \; cm^{-1}/K$.

For the simplest molecules, the line strength S_{0j} and the lower-state energy E" can be computed from first principles. For more complex molecules such as water vapor, direct calculation is more difficult and experimental measurement is required for accuracy. These physical constants (and others related to absorption line broadening) are tabulated in extensive databases such as HITRAN (3) and BT2 (4). Once these physical constants have been determined to the required accuracy, they allow determination of molecule absorption depending only on temperature, pressure and molecule concentration. Apart from electronic or other malfunction that can be identified with suitable sensor health monitors, there are no other factors that might drift with time and change measurement results.

Semiconductor diode lasers can be tuned rapidly by changing forward current, providing a convenient method of mapping out gas absorption vs wavelength. Distributed feedback (DFB) lasers developed for telecommunications are particularly suitable because they are highly reliable and tune without mode hopping: laser wavelength is a repeatable, single-valued function of temperature and current. Figure 3 shows how light from a DFB laser transmits near 1400 nm through 30 mm of air containing approximately 0.4% water vapor. There is an overall modulation of DFB laser output as shown by the dashed line. When light transmission through the 30 mm path (the thin solid line) is divided by the DFB laser output modulation, three absorption peaks are seen.
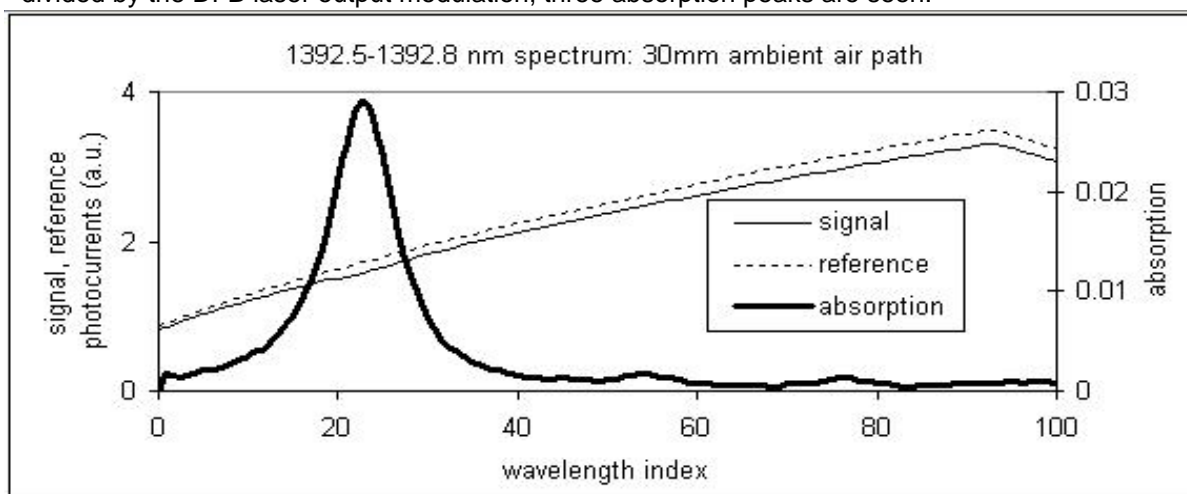
Figure 3: light absorption by water vapor near 1393 nm

Detailed knowledge of the spectral constants for these absorption lines allows one to calculate temperature, pressure and water concentration along the path, subject to assumptions about the uniformity of gas conditions along the path. Scanning over multiple absorption lines can provide information on the nonuniformity along the path.

Absolute measurement of light transmission is difficult because many factors not related to the target gas will change the measurement result. Particulates, beamsteering due to turbulent flow, vibrations of optics and other factors will all affect light transmission. These perturbing factors do not correlate with laser wavelength like molecular absorption, however. By repetitively scanning wavelength at high speed, light transmission changes due to gas absorption can be distinguished from light fluctuations due to noise sources. Figure 4 shows an example.
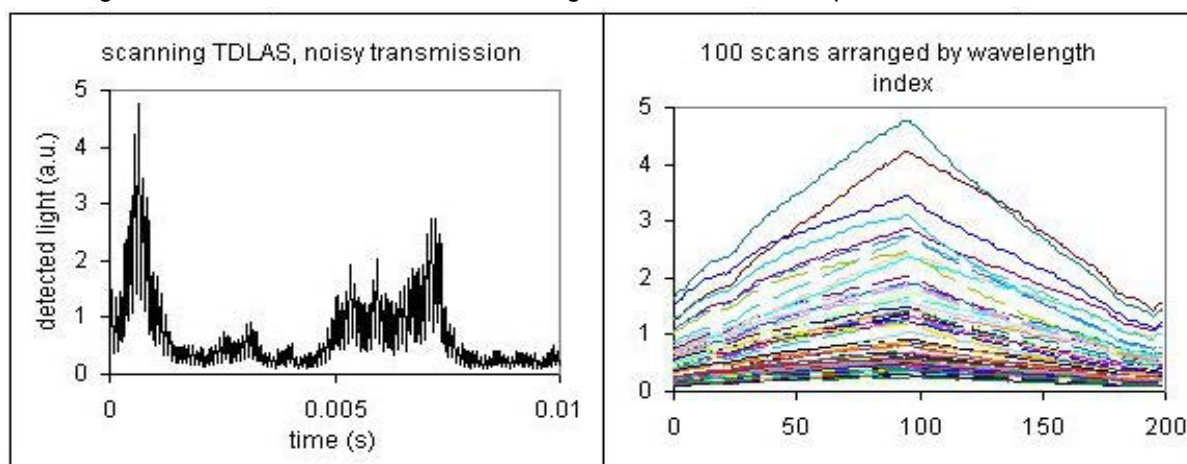
Figure 4a: detected light fluctuation during laser scanning
Figure 4b: column-averaging to suppress noise

Figure 4a depicts light transmission fluctuating over a 10-millisecond measurement time. Superimposed on the noisy transmission is the rapid scanning of the laser in power and wavelength. If we re-arrange the transmission data into a sequence of scans as in Figure 4b, some scans are strong and others weak but nearly all scans show the same basic shape or wavelength dependence. Averaging these scans together we generate a plot of light transmission vs wavelength with most of the transmission noise suppressed, shown in Figure 4c. By dividing out the laser amplitude modulation and taking the logarithm, we derive the absorption spectrum.
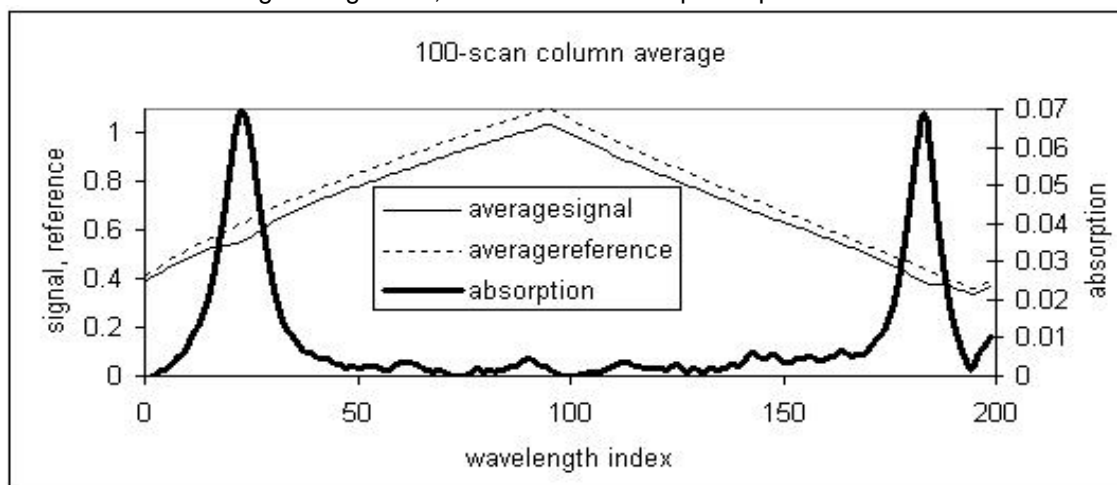
Figure 4c: column-averaged absorption spectrum, 1395.45 - 1395.75 nm

As long as the laser scanning rate is faster than the light transmission fluctuations due to technical noise sources, this form of scanning and averaging is very effective at measuring small absorption signals in noisy environments. The technique has many of the strengths of modulation spectroscopy as discussed below.

While the principles underlying TDLAS are as old as the laser, practical TDLAS sensors had to wait for light sources, optics and electronics developed for telecommunications. Today's DFB lasers are robust, predictable and reliable components unlike tunable lasers in prior years. Optical fibers allow the routing of light like electrical signals, meaning that critical optical alignment is required only along the gas path of interest. Related fiber optic components such as couplers, splitters and multiplexers allow light signals to be divided and combined as readily as electrical signals. InGaAs detectors allow high-speed, low-noise light sensing across a wavelength range from 800 nm to beyond 2000 nm, the desired range for many gas absorption lines of interest.

3.0 PRIOR DEVELOPMENTS

TDLAS has been applied to air-breathing engine research in a number of projects. Southwest Sciences Inc. and Zolo Technologies have developed sensors to be flown aboard HIFiRE 1 which will sense oxygen concentration and velocity in stratospheric air passing outside the HIFiRE payload during vehicle re-entry.(5) Physical Sciences, Inc., in cooperation with Stanford's High Temperature Gasdynamics Laboratory, has also developed combustion sensors intended for harsh engine conditions (6). PSI has also miniaturized TDLAS instrumentation (7) and applied TDLAS in several ground test facilities (8).

In addition to an oxygen sensor for HIFiRE 1, Zolo has applied TDLAS to military aircraft turbine engines (Figures 5 and 6) as well as the high-enthalpy LENS II shock tunnel at CUBRC and the arc-heating facility at NASA-Ames. The main component of Zolo's business is monitoring coal combustion, which entails passing a laser beam through the combustion zone of a coal boiler. In all of these situations the harsh environments severely limit the types of sensors that can be employed.
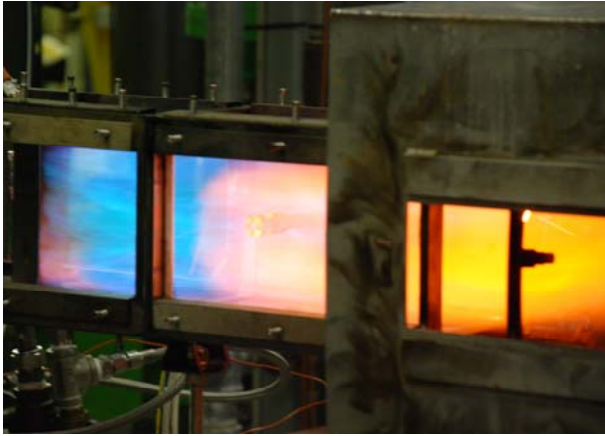
Figure 5: in-situ combustion sensor   **Figure 6: turbofan exhaust sensor**

4.0 REQUIREMENTS FOR ON-BOARD TDLAS COMBUSTION SENSOR

Exhaust gases from a scramjet combustor will contain roughly 10% water concentration at temperatures from 1000 K to 2500 K. For use in monitoring supersonic combustion, a sensor must be able to report temperature and concentration with sensitivity near 20 K and 0.5%, respectively. For a small-scale combustor with 100 mm duct width, this implies sensitive measurement of a few percent peak light absorption. Uncertainty in light measurement due to detector noise and all other sources must be well below this level.

For in-flight sensing, all electronics, optics, and fiber optics must be compact and rugged enough for flight. Typical requirements will be an operational range from 0 C to 70 C, vibration tolerance greater than 10 g up to 2000 Hz, and tolerance of pressure changes from 1 atmosphere to vacuum.

The requirements on the fiber optic components and optics which must deliver light into the combustor are much more severe. The optics which collimate light exiting a fiber will be mounted to walls whose temperature may exceed 900 K. These optics must maintain alignment to a few milliradians during the temperature excursions and in the face of vibrations and thermal warpage.

Finally, the key sensor information (temperature and concentration) must be reported at rates high enough to track combustion changes, perhaps up to 100 measurements per second. To conserve limited telemetry bandwidth, it is ultimately preferable to report processed rather than raw data, implying that the sensor must perform real-time processing.

5.0 TDLAS DESIGN CHOICES

At the most basic level, the TDLAS sensor package must survive and function during the sounding rocket flight. This dictates the size, weight, power consumption and ruggedness required of the design. Subject to these requirements, the sensor must measure gas properties as sensitively as possible.

In order to yield the highest sensitivity to temperature, concentration and the other gas properties of interest, this means making the sensor as sensitive to light absorption as possible. Depending on concentration, temperature and the specific absorption line chosen, peak light absorption may vary from greater than 90% to below 0.1% and the sensor must faithfully measure over this range. Best sensor performance means lowest minimum measurable absorption.

5.1 Derivation of Temperature and Concentration from Spectra

Appendix A outlines the derivation of a molecular absorption spectrum from the transmission of light through a gaseous medium. Specializing to a spectrum containing just two absorption lines and assuming uniform temperature, pressure and concentration, we have:

$$\alpha_{tot}(\nu) \ = \ P \ L \ x \ [S_1(T) \ g_1(\nu, T, P) + S_2(T) \ g_2(\nu, T, P)]$$

Our task is to fit a function of laser detuning for the parameters P, x, and T which we wish to know. We are likely to have fit parameters as well for a quadratic baseline. Hence in all we have a 6-parameter fit. From this fit we can determine the absorption areas of each of the two lines, which are defined in terms of just a few quantities:

$$A_i \ = \ P \ x \ L \ S_{0i} \ [Q(T) \ T \ / \ Q(T_0) \ T_0] \ exp[-c_2 \ E_i" \ (1/T - 1/T_0)]$$

where P is pressure in atmospheres, x is water concentration (mole fraction), T is absolute temperature and the remaining quantities are the standard spectroscopic constants. The ratio of the two absorption lines:

$$R \ = \ A_2 \ / \ A_1 \ = \ [S_{02}/S_{01}] \ exp[-c_2 \ \Delta E" \ (1/T - 1/T_0)]$$

depends only on spectroscopic constants and absolute temperature. We then invert the function to determine temperature:

$$T \ = \ c_2 \ \Delta E" \ [c_2 \ \Delta E"/T_0 + ln(S_{02}/S_{01}) - ln(A_2/A_1)]^{-1}$$

With temperature thus determined and pressure determined from the Voigt-profile fits of the absorption line shapes, we then determine the water vapor concentration:

$$x \ = \ A_i \ / \ [P \ L \ S_{0i} \ \{Q(T_0) \ T_0 \ / \ Q(T) \ T\} \ exp\{-c_2 \ E_i"(1/T - 1/T_0)\}]$$

(We can compute the concentration from either of the two absorption areas or, preferably, use the weighted average of the two.)

Assuming we know the spectroscopic constants, our temperature uncertainty is set by our absorption uncertainty, δA. For the purpose of estimating the uncertainty, the error in the integrated absorption is related to the error in absorption at a specific frequency, $\delta\alpha$, by the absorption line width $\Delta\nu$:

$$\delta A \ = \ \Delta\nu \ \delta\alpha$$

The absorption error $\delta\alpha$ depends on instrumental noise sources and is constant across the spectral range. Taking the derivative of our expression for temperature and performing some algebraic manipulations:

$$\delta T \ = \ [T^2/c_2 \ \Delta E"] \ [-\delta A_1/A_1 + \delta A_2/A_2]$$

(where it's understood the errors $\delta A_i/A_i$ should be added in quadrature if they're not correlated)

For our uncertainty estimates, we approximate the absorption areas A_i by $A_i = \alpha_{pki} \ \Delta\nu$ and assume comparable absorption widths for the two lines, letting us re-write the uncertainty as

$$\delta T \ = \ [T^2\Delta\nu \ \delta\alpha/c_2 \ P \ x \ L \ \Delta E"] \ [-1/S_1(T) + 1/S_2(T)]$$

or

$$\delta T \ = \ [T^2 \ \delta\alpha/c_2 \ \Delta E"] \ [-1/\alpha_{pk1}(T) + 1/\alpha_{pk2}(T)]$$

(We note again that the absorption strengths or peak absorptions are to be added in quadrature for random noise sources, while common-mode noise sources between the two lines are partially suppressed in the temperature uncertainty.)

The concentration uncertainty δx is computed along similar lines. If the spectroscopic constants are known then the fractional concentration error is proportional to the fractional absorption error.

The temperature uncertainty formula tells us two important things: first, we have limited options to improve temperature sensitivity beyond choosing an absorption line pair with the highest strengths and the largest lower-state energy difference and, second, sensitivity degrades very rapidly with temperature.

Among the things we can control is our absorption sensitivity $\delta\alpha$. For a production aeropropulsion system with fiber connections shorter than 50 meters (to limit modal noise), 0.1% is realistic in the absence of transmission noise. In a highly turbulent environment such as a jet turbine interior, transmission noise may be high and averaging times up to a second may be required to reach the needed sensitivity.

5.2 Classifying Error Contributions

Design of the Zolo sensor was dictated by minimization of temperature and concentration uncertainties. Table A-1 lists the error sources of concern, classified according to our ability to correct for the errors. The TDLAS part of the HIFiRE 2 experiment will generate several seconds of spectroscopic data to be relayed to the ground for post-processing; there is no opportunity to repeat the experiment for years (if ever). If the quality of that data is poor due to excessive noise caused by flow turbulence or optics vibration, then there is little that can be done in post-processing to recover useful spectroscopic information. Likewise, excessive detector noise or shot noise are fundamental and not correctable.

Systematic errors such as a wavelength scale error or inaccurate spectral constants are in a different class. Spectral constants can be re-measured to improve accuracy and the telemetered data set re-analyzed with the new constants. The wavelength scale can be inferred from the locations of the absorption peaks, as long as the telemetered data is of high enough quality. Therefore these error sources can be corrected in post-processing.

These considerations led to the design of a sensor with minimum contributions from the un-correctable errors. The errors of greatest concern were the following:

shot noise

This noise source depends on the absolute detected photocurrent level, including radiant background light. This noise source will dominate if the collected light is low and background light is high. This is a white noise source, constant at all frequencies.

detector noise

Detector noise will dominate at the lowest detected light levels. This noise source can be reduced by careful photodiode/amplifier design. For Zolo's sensor, the detector noise is 0.005 nanoamp per square-root Hz. Like shot noise, it is largely independent of measurement frequency.

light transmission noise

Flow turbulence or vibration of the send/receive optics will lead to fluctuations in the amount of collected light, and this is often the dominant noise source in combusting flows. In many cases turbulence noise follows a 1/f spectrum, with much larger fluctuations occurring at lower frequencies. Based on previous measurement campaigns carried out in combusting flows, we estimate a noise density below 0.05% per square-root Hz near 10 kHz, following a 1/f spectrum from below 1 kHz to above 500 kHz. Transmission noise is multiplicative; to determine the absolute noise contribution we multiply by the detected signal strength. Multiplicative noise sources will dominate at high signal strengths and will become negligible at low signal strengths.

Light transmission noise may be dominated by mechanical vibrations of the send and receive optics; in this case, noise might be overwhelmingly large at unintended mechanical resonances. The design of the optics, fibers and detectors in the Zolo sensor was dictated by the need to minimize the effect of vibrations and acoustic noise on the optics. In particular, the send and receive optics' focal lengths were chosen to tolerate large angular deviations of the beam paths and the receiving fibers' core diameters were increased to 200 micrometers to maximize the amount of light captured.

laser noise
The laser's power or center wavelength may fluctuate. Laser amplitude noise is a multiplicative noise source which must be combined with light transmission noise. The intrinsic noise of the DFB lasers used in Zolo's sensor is very low; the relative intensity noise is less than 10^6 and intrinsic frequency fluctuations are below 3 MHz, or 0.1% of the widths of the absorption lines to be measured. The dominant cause of laser noise is noise and instability of the current driving the DFB laser. Careful electronic design keeps the current noise and stability below 5 microamps, at which point laser noise is far smaller than the expected light transmission noise.

quantization noise
When attempting to discern small absorption dips on small optical signals, bit noise may be an issue. In the Zolo sensor the bit noise is kept very small by using 16-bit digitizers and by averaging 1000 scans together per measurement. These steps keep the bit noise contribution to absorption noise below 0.1% of the peak absorption even under worst-case conditions (signal level below 10% of the full range, peak absorption below 1%).

preventable electronic faults
There is risk of un-correctable noise or distortion from electrical pickup, cross-talk and detector saturation. These error sources are difficult to quantify but can be minimized by careful electrical design; for example, noisy electronics and quiet electronics may be isolated in separate enclosures with careful attention paid to grounding and shielding.

modal noise and interference fringes
For small absorptions, these multipath interference sources can be dominant. Because the interference leads to systematic distortion of the spectra, the effect on measurement results can be much more damaging than random noise.

Of the listed error sources, the first four cannot be made negligible over the full range of conditions possible during the HIFiRE 2 experiment, while the last three can be made small enough to be harmless by careful sensor design. The signal/noise model discussed below accounts for the first four to guide detailed sensor design.

5.3 Spectral Selection
The first step in TDLAS sensor design is choice of an appropriate wavelength range for the intended measurement. The goal is to interrogate a set of absorption lines whose relative and absolute absorption strengths can lead to a sensitive determination of temperature, concentration or other quantities of interest. Zhou (9) describes a set of design rules which lead to optimal wavelength choices. There are three key requirements:
    1) The chosen wavelength range must contain several absorption lines with different temperature dependences (i.e., different lower state energies E").
    2) The target absorption lines must have peak absorption strengths between 5% and 90% over the nominal range of temperature, pressure, concentration and path length in the application.
    3) The target absorption lines must be isolated well enough to allow the desired gas quantities to be calculated from the measured absorption spectra.
    Researchers at the Air Force Research Laboratories have identified spectral ranges suitable for scramjet combustion monitoring. The chosen range is near 1396.5 nm and is shown in Figure 7. In this range are four distinct absorption peaks covering a range of lower state energies. This will enable sensitive calculation of temperature and concentration.
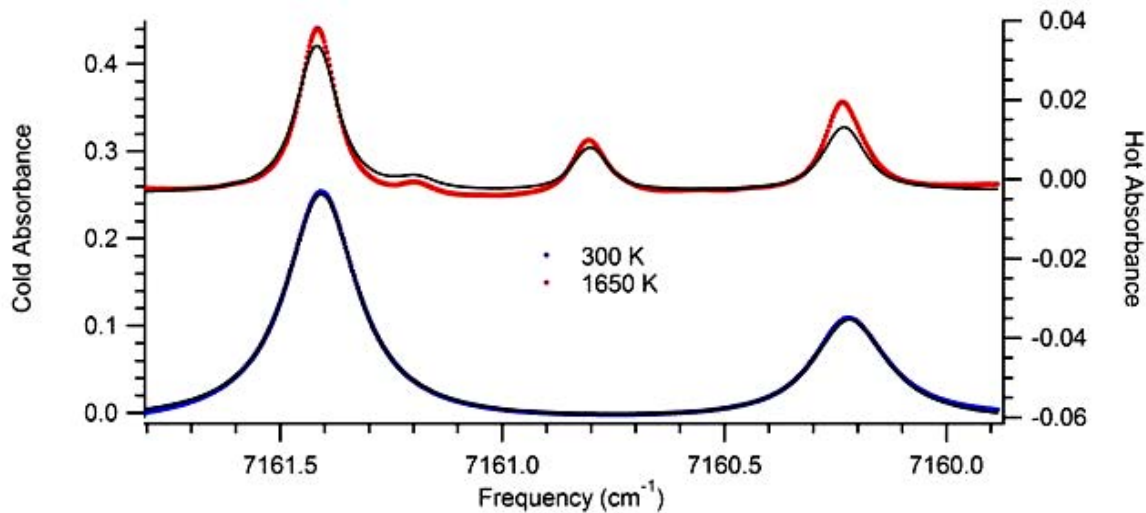
Figure 7: Target spectral range

5.4 Maximizing Sensitivity to Light Absorption

Given a set of absorption lines, the aim is to measure their absorption strengths as accurately as possible. To achieve the highest absorption sensitivity, we must control all causes of detected light level changes other than absorption by the molecule of interest.

Achieving high absorption sensitivity has been studied extensively since the advent of conveniently-tunable lasers. A variety of measurement methods such as wavelength- and frequency-modulation spectroscopy have been applied to overcome various confounding noise sources. Silver (10, 11) reviews these choices and quantifies their relative merits. In general, modulation greatly reduces sensitivity to low frequency noise and in many cases allows a TDLAS experiment to reach fundamental limits.

Modulation spectroscopy detects modulation of light transmission at the laser modulation frequency and selected harmonics (6). This technique reduces contributions of transmission noise due to gas turbulence but comes at a price. The modulated signal is challenging to interpret and relate to the fundamental molecular absorption of interest; the signal depends on the modulation depth, the widths of the target gas absorption lines (and, hence, on pressure and temperature), and on the absorption depth (12). A practical sensor based on modulation spectroscopy may be limited in pressure, temperature and concentration range to a limited space in which modulation spectra can be interpreted accurately.

A more direct measurement of molecular absorption may be preferable to achieve high accuracy in a practical sensor, particularly when probing complex spectra (multiple absorption lines with differing strengths) in environments with highly variable temperature, pressure and concentration. Direct absorption measurement also allows more straightforward measurement and control of systematic errors due to parasitic etalons and fiber modal noise.

A powerful direct method is Balanced Ratiometric Detection (13), which can achieve performance comparable to modulation spectroscopy in analog electronics. This approach compares light transmission through a path of interest to a reference light level proportional to laser output. Using low-noise, high-speed detector electronics, fluctuations in laser intensity may be divided out very accurately, yielding actual light transmission through a path of interest. When transmission fluctuations along the path of interest are the dominant noise source, however, removing laser intensity fluctuations alone cannot improve the measurement performance. The effect of transmission noise must be suppressed, most commonly by increasing modulation frequency to be well above the frequency of the transmission noise.

With high-speed analog-to-digital converters and microprocessors it is now feasible to apply direct measurement of molecular absorption even in noisy environments. DFB lasers may be scanned repetitively over target absorption lines at rates greater than 10 kilohertz, above most technical noise sources. The scans may be averaged to derive absorption spectra with quality comparable to what can be achieved with modulation spectroscopy. This is the approach chosen for the Zolo sensor.

Direct scanning and averaging has the advantage of faithfully recording absorption spectra with fewer interpretation issues. A wide range of absorption strength and line broadening can be handled, allowing complex, multi-line spectra to be probed. The cost of this versatility is that high-speed A/D conversion and real-time computation are required; the Zolo sensor must process 80 megabytes of data per second to derive absorption spectra.

5.5 Fundamental Noise Limits: Random Noise

Our minimum detectable absorption is set by the total noise at our detector input divided by the detected light signal. System design thus attempts to maximize detected light and minimize noise. Figure 8 sketches the contributing factors. By efficient optical design we strive to deliver and collect as much light as possible. Minimizing noise involves a number of design trade-offs. Expressed in amperes of photocurrent, the total noise will be comprised of detector noise, shot noise, and multiplicative noise (light transmission noise and laser noise).

$$\delta a$$
$$n_{TOT} / [I_s \, t_{eff}^{1/2}]$$

t_{eff}
$t \, f_{comp} \, f_{spec}$

n_{TOT}
$[\Sigma \, c_i \, n_i^2 / \Sigma \, c_i]^{1/2}$

I_s
$R_{det} \, P_L \, \eta_{int} \, \eta_{probe} \, e^{-2 \, \alpha \, L}$

f_{spec}
$<FWHM>/range$

n_i
$[n_{det}^2 + n_{shot}^2 + n_{multi}^2]^{1/2}$

c_i
$c_0 \, [exp(-1.667 \, <FWHM>/range)]^i$

η_{probe}
$k \, R_s \, [w_c / \Delta\theta \, L]^2$

n_{det}
$f \, n_{d0} / f_0$

n_{shot}
$[2 \, e \, (I_s + I_{bkg})]^{1/2}$

n_{multi}
$(n_{m0} \, f_0 / f) \, I_s / i$

range
$1.5e7 \, |1/\lambda_c - 1/\lambda_h|$

FWHM
$0.5346 \, \gamma_c + [0.2166 \, \gamma_c^2 + \gamma_D^2]^{1/2}$

γ_c
$2 \, P \, (x \, \gamma_{self} + 0.81 \, \gamma_{air})(T_0/T)^n$

**Figure 8: Contributions to light absorption uncertainty**

For a given detected light level, shot noise sets the performance achievable. Noise generated in the detector and associated electronics can be reduced to approach the shot noise limit by careful design but in general lower detector noise implies reducing detector bandwidth. On the other hand, fluctuations in light detected after transmission through a turbulent medium tend to have larger amplitude at lower frequencies; in the kilohertz-to-megahertz range of interest to us, the noise typically has a 1/f spectrum. The effects of transmission noise on the absorption measurement are thus minimized by scanning faster, therefore requiring higher detection bandwidth. For a given amount of detected light and transmission noise, there will be an optimum detector bandwidth.

Given an optimum detector bandwidth we choose the rate at which the laser is scanned so that the target absorption spectrum takes up that signal bandwidth. In an environment such as a scramjet combustor the detected light level is high and so the optimum scanning rate is also high, sometimes beyond 10 kilohertz. Wavelength-scanning an industry-standard telecom laser beyond 10 kHz is challenging because the wavelength shift with drive current is primarily a thermal response and so progressively greater drive current modulation is required to scan laser wavelength faster than 10 kHz.

In order to make optimum design choices, we model a basic water absorption spectrum and consider how various noise sources affect how we measure it. In Figure 9 we graph two typical absorption lines scanned at 50 kHz. The absorption lines' heights and widths will depend on temperature and pressure, and detector bandwidth must be high enough to resolve the narrowest spectral features of interest. In the example, detector bandwidth must exceed 2 MHz to faithfully record the absorption lines, and the sampling rate is 10 megasamples per second. This is adequate (barely) for the absorption features shown.
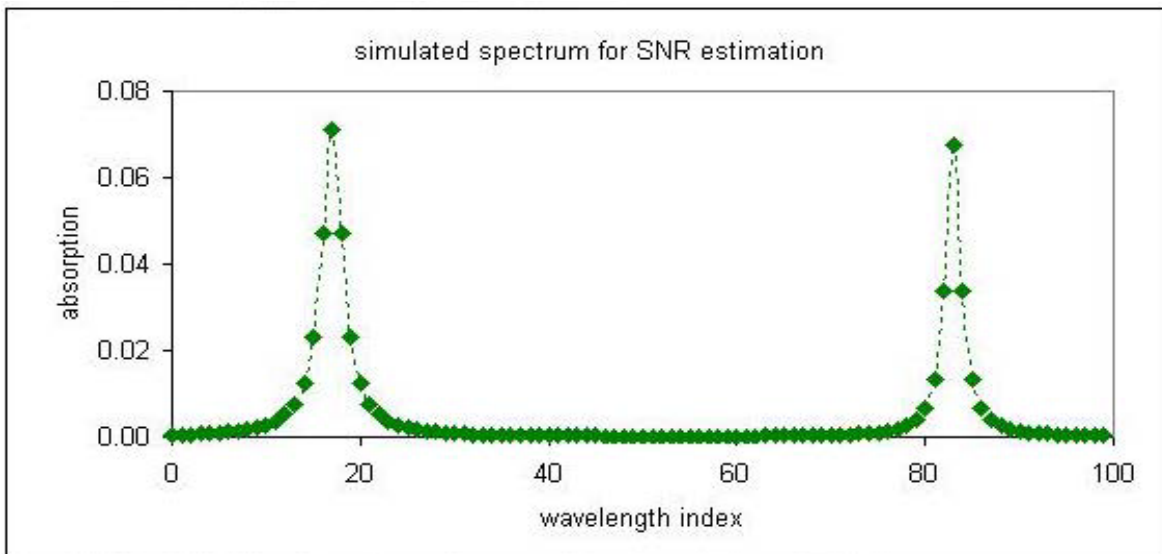

Figure 9: simulated two-line absorption spectrum for noise calculation

A proper accounting of noise contributions must reflect the frequency content of both the absorption spectrum being scanned and the noise sources. A Fourier transform of the repetitively-scanned spectrum in Figure 9 leads to a series of peaks at harmonics of the scanning frequency. The amplitudes of the peaks drop off with frequency, with the steepness of the drop-off depending on the ratio of the absorption line widths to their separation. For peaks separated by many absorption widths as in Figure 9, there is significant signal content up to ten times the scanning frequency. For absorption peak separations not much larger than the line widths, the signal content is contained in just the first few harmonics of the scanning frequency.

While the signal to be detected has frequency content dependent on the scanning frequency and peak separation, the noise also has a frequency dependence. Detector noise will be roughly constant at all scanning harmonics up to the detector bandwidth while light transmission noise will generally follow a 1/f distribution. To determine the total noise n_{TOT} in a column-averaged spectrum, we must sum up the noise at all scanning frequency harmonics, properly weighted by the signal constant at each harmonic.

Appendix C displays the input quantities involved in estimating measurement performance assuming different detected light and background light levels, different detector and turbulence noise levels, different scanning frequencies and different temperatures, pressures and absorption path lengths. The first column lists the spectral constants and relevant gas conditions while the second column lists the parameters specific to the Zolo sensor. With these constants as inputs to the formulas in Figure 8, we estimate sensor performance under various conditions with different design choices.

With the sample absorption spectrum in Figure 9 we can see how absorption uncertainty scales with scanning frequency (Figure 10). At lower scan rates transmission noise dominates while at higher scanning frequencies detector noise dominates. There is a broad minimum near 100 kHz. This optimum point moves to lower frequencies as signal strength drops and moves to higher frequencies as transmission noise rises. Assuming a scanning rate of 50 kHz, Figure 11 shows how absorption sensitivity depends on detected signal strength. Absorption uncertainty rises to 1% at 0.01 microamp, which is much smaller than expected signal strength. Hence we have a wide performance margin.
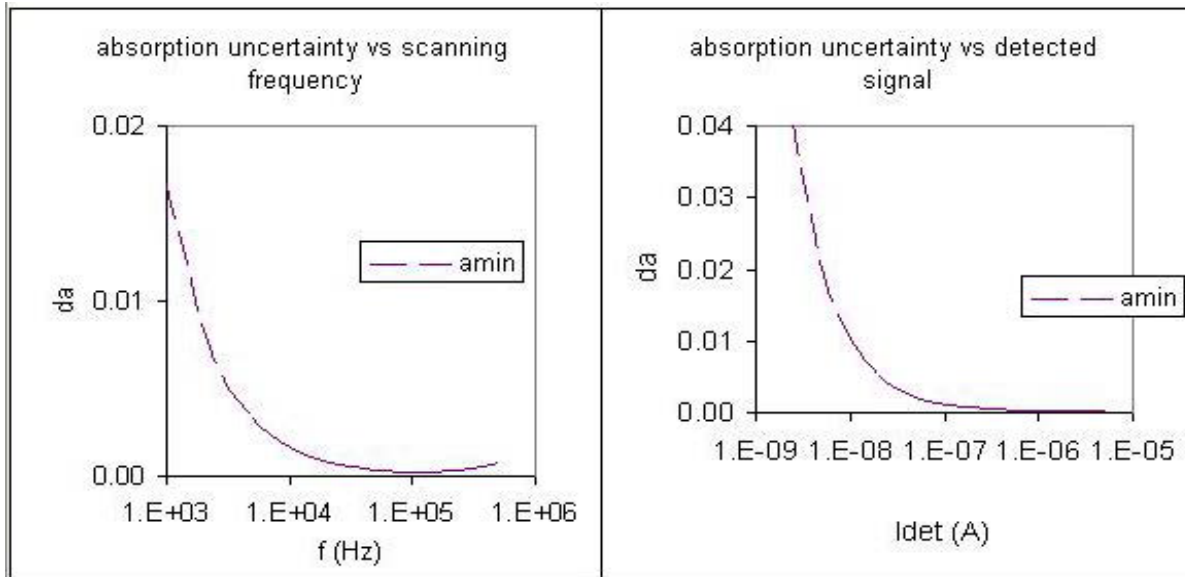
Figure 10: scan frequency dependence   Figure 11: detected light dependence

When translating from an absorption spectrum to gas temperature and concentration, sensitivity is greatly reduced, particularly at higher temperatures. Figure 12 graphs temperature uncertainty against temperature. For sensitive temperature measurement, absorption sensitivity must be quite high.
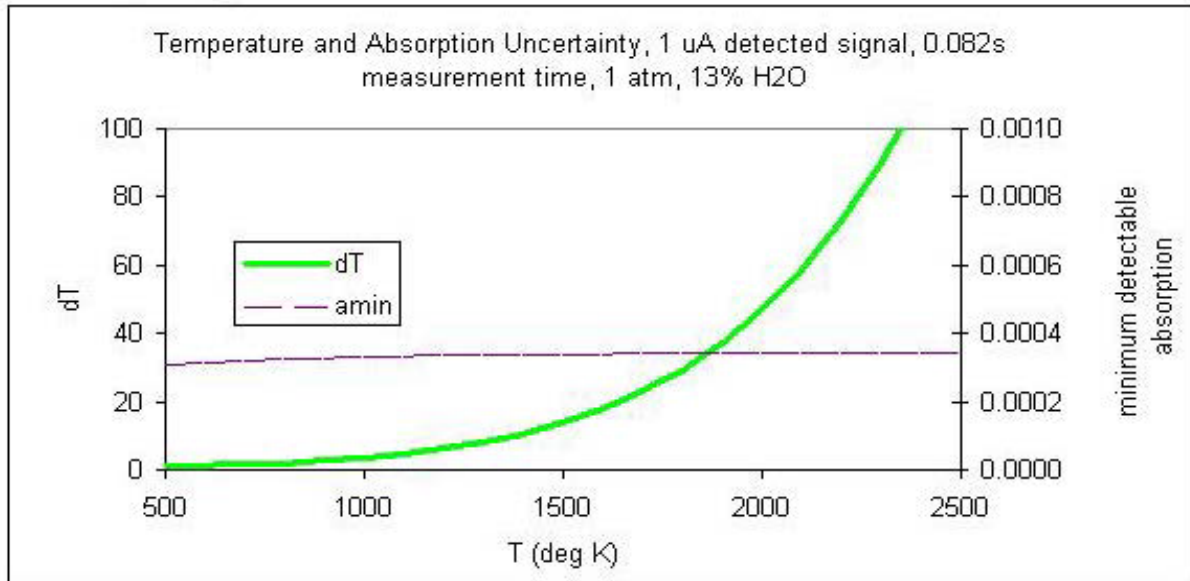
Figure 12: temperature measurement uncertainty vs temperature

5.6 Multipath Interference Noise Sources

It is inevitable that light from the laser can take more than one path through the sensor's optical system to reach the detector. If this happens then the detected light level will change due to constructive and destructive interference between light taking different paths. This interference will change depending on optical path lengths (and, hence, on temperatures and stresses along fibers) and on laser wavelength. The dependence on laser wavelength is a severe problem: an intensity fluctuation due to interference will look like a molecular absorption feature and will not average out as transmission and detector noise will.

There are two key sources of multipath interference in a TDLAS sensor. The first source is multiple reflections resulting in parasitic etalons. Reflectors inside optical fiber components or elsewhere that are separated by 5 to 20 cm will lead to interference fringes in the detected light with a frequency spacing comparable to the widths of the target absorption lines. Since it is the amplitude and not the intensity of the interfering light that is important, even very small reflections can be a problem. For example, two 0.1% reflectors will lead to intensity ripples of 0.4% peak-to-peak, enough to obscure small absorption lines.

A second type of multipath interference is fiber optic modal noise. A multimode fiber can support hundreds or thousands of spatial modes, and these modes propagate down a fiber at different velocities. At the end of a length of fiber, all of the modes interfere to produce a complex speckle pattern. The speckle pattern changes with laser wavelength, fiber temperature, light launching conditions, etc. While the total power in the speckle pattern is constant, any mode-dependent loss that obscures part of the speckle pattern (for example, an imperfect fiber connection) converts changes in the speckle pattern into changes in the detected light.

Mitigation techniques are limited. The first line of defense against parasitic etalons is to minimize all unwanted reflections along the optical path. Optical surfaces such as fiber endfaces and detectors are tilted and antireflection coated. Windows are wedged to eliminate multiple reflections. Components like fiber splitters are designed for minimum return loss (or back-reflection). When all of these steps are taken, parasitic etalons can be limited to below 0.05% peak-to-peak. Going lower than this becomes progressively more difficult.

Techniques to reduce fiber modal noise are even more limited. Mode-dependent losses from imperfect connectors or imperfect collection of light onto the detector surface can be reduced by careful design. Keeping multimode fiber lengths short helps by increasing the spacing between modal noise "fringes" to make it easier to distinguish noise from absorption lines. Fibers designed for low loss and low mode dispersion reduce modal noise effects similar to keeping fiber lengths short, but such fibers are not available in all core sizes.

In a carefully-designed TDLAS sensor, multipath interference is often the performance-limiting factor. Figure 13 shows an example. The black curves plot light transmission across an 11-cm air path transmitted through 150 meters of GIF50 multimode fiber, while the green curves show the absorption spectra derived. As mode-dependent loss is introduced by loosening an FC/APC connection following the multimode fiber, transmission drops by just 2 dB while the noise on the absorption spectrum rises from less than 1% peak-to-peak to more than 16% peak-to-peak.
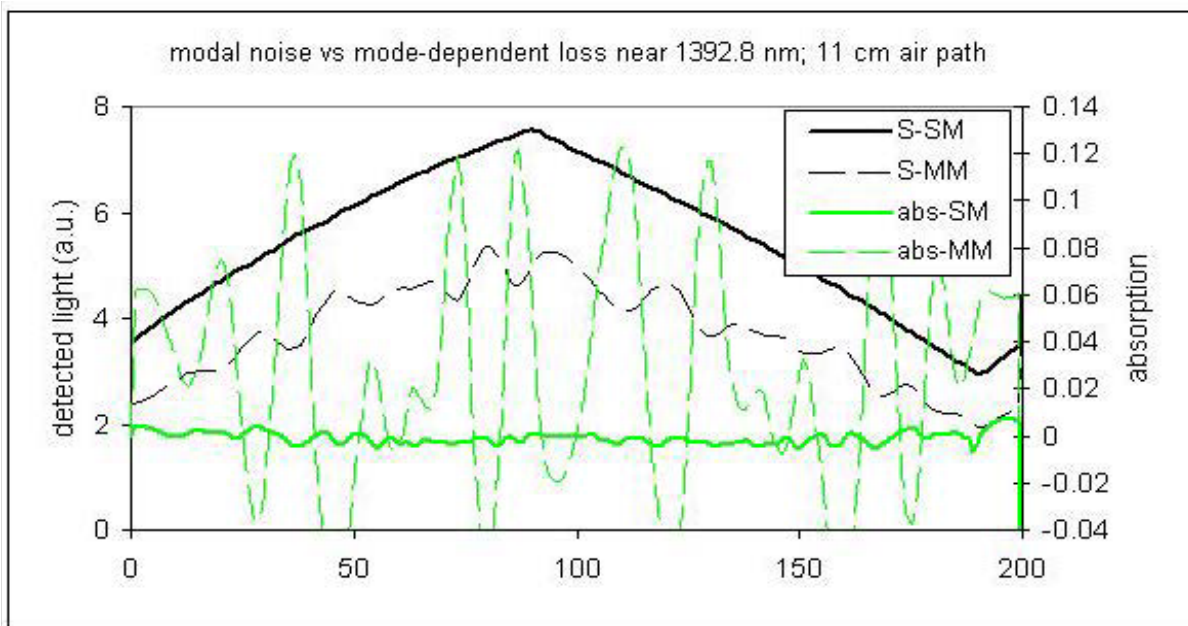
**Figure 13: multimode fiber modal noise**

5.7 Total System Performance

Under nearly ideal laboratory conditions absorption sensitivity levels far below parts per million have been demonstrated (14), but it is challenging to achieve this in deployed sensors. The use of optical fibers to route light between sensitive electronics and probe locations is a key feature of a practical sensor but systematic noise sources such as parasitic etalons and modal noise lead to much higher total absorption noise. An overall absorption sensitivity between 0.01% and 0.1% can be achieved with care, and this practical limit sets the level to which detector noise and transmission noise need to be reduced. Since the systematic errors are not random and do not average to zero, there is a limit to the useful measurement time, set when uncertainties due to random errors are averaged down to the level of the systematic errors. This takes tens of milliseconds for the Zolo sensor.

The key aim of Zolo's sensor development project has been to optimize all aspects of the design for highest absorption sensitivity while delivering a flight-worthy package. This has driven the design compromises that have been made.

6.0 ZOLO ARCHITECTURE

Zolo's sensor architecture is shown in Figure 14. The system is a compromise between capability and compactness. The system contains a single DFB laser which limits the number of absorption features that can be probed. We maximize the laser scanning range to make up for this.
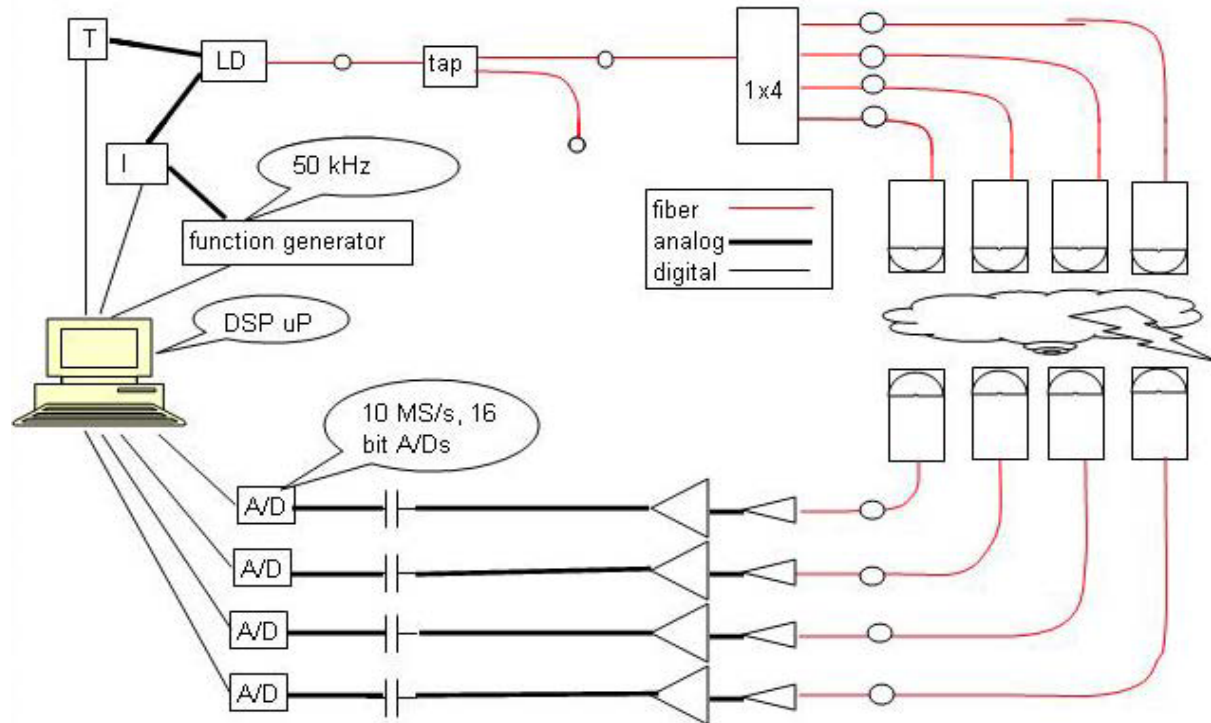
Figure 14: Zolo sensor architecture

The system routes light to four paths and collects and detects the optical signals. The signals are digitized at a rate of 10 million samples per second with 16-bit resolution. The sensor includes a field-programmable gate array (FPGA) for rapid averaging of the data signals, after which data is routed to a digital signal processor (DSP) for on-board data analysis. The resulting averaged signals are transmitted to the host computer via RS-485 for telemetry to the ground. To minimize the risk of data loss, the photodetector currents are also provided as buffered analog outputs, to be collected and digitized separately by the sounding rocket host computer for telemetry to the ground.

The physical realization of the architecture includes two printed-circuit boards, fiber optic couplers and splitters, a DFB laser and four detectors. All components must meet NASA's sounding rocket requirements individually and as a system. Figures 15 and 16 show the sensor package.
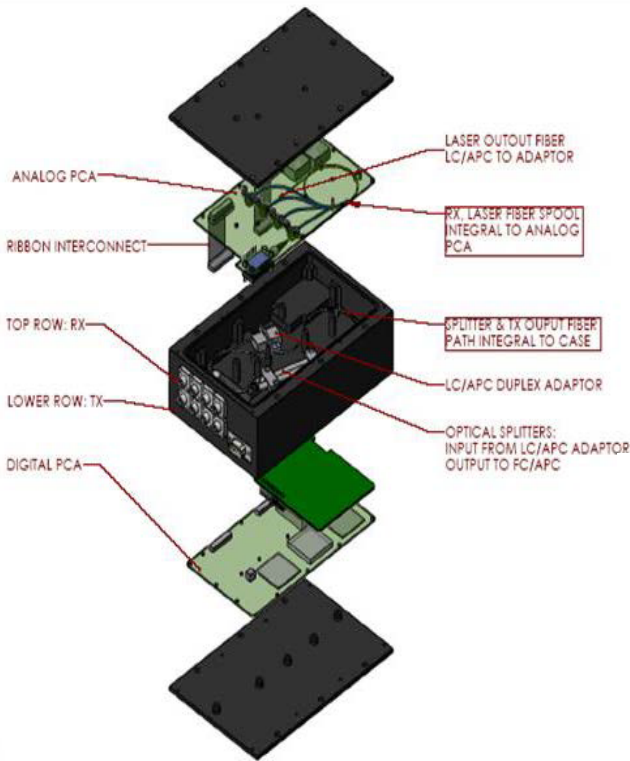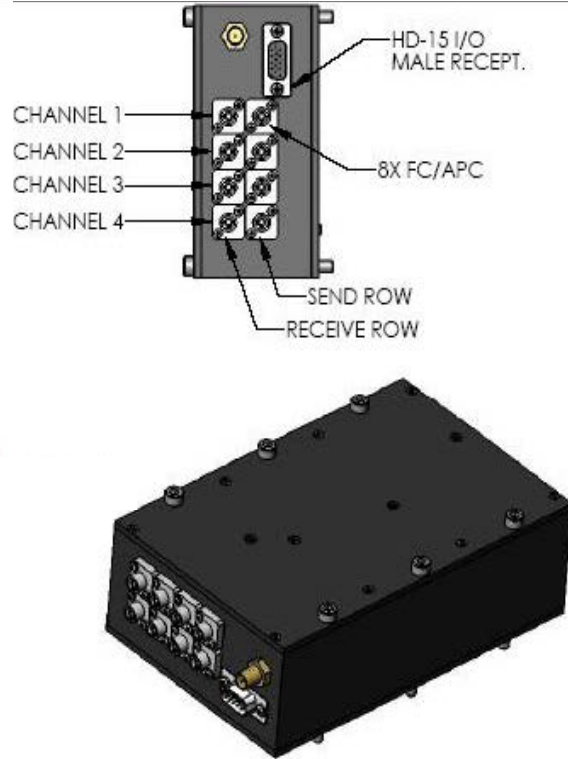
Figure 15: exploded view

Figure 16: sensor outline and mounting

7.0 DESIGN DETAILS

7.1 Laser and Drive Electronics

To maintain a stable output wavelength, the DFB laser must be temperature-controlled with an accuracy better than 0.1 C over the specified ambient range of 0 to 61 C. Laser drive current is modulated at 50 kHz in a programmable waveform chosen to achieve linear scanning of wavelength. Since current scanning causes wavelength to change primarily by thermal effects, fast, linear wavelength scanning requires a large and highly nonlinear driving waveform. Figure 17 graphs the amplitude and wavelength waveforms in black and green, respectively. The laser output power follows the current waveform closely. The current waveform is generated by the FPGA and is programmed to achieve a near-linear change in frequency with time.
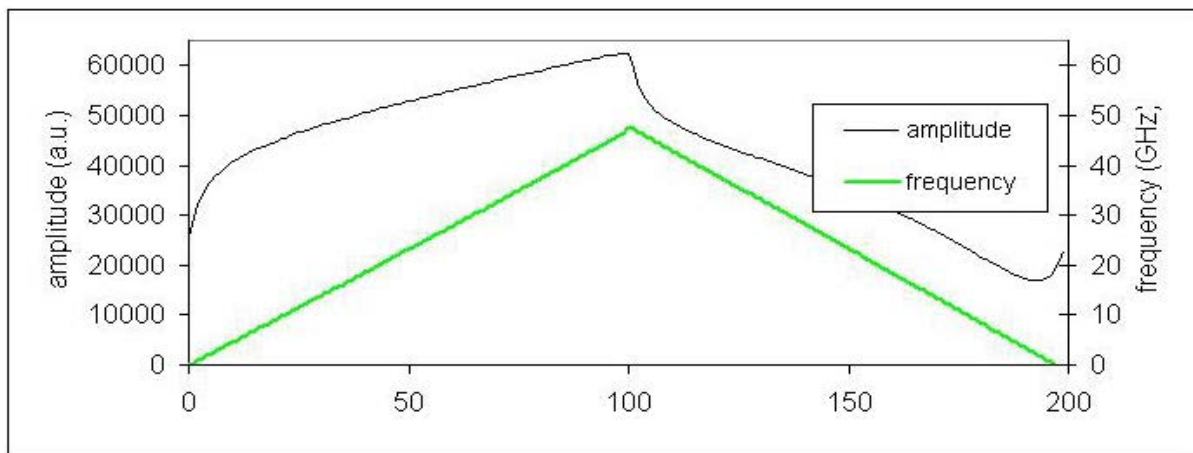

**Figure 17: laser power and wavelength scanning waveforms**

7.2 Fiber Couplers

The Zolo sensor uses two fused fiber couplers. The first is a 2x2 tap which attenuates the strong laser output to a level that will not saturate the InGaAs detectors. (For low-light conditions, it is easy to switch to the high-transmission leg of the tap.) The second is a 1x4 splitter. These couplers meet stringent Telcordia ruggedness requirements but are highly susceptible to mechanical vibrations at tens of kilohertz.

7.3 Collimator Optics

The collimators must send light into the scramjet duct and collect as much of the transmitted light as possible. Light is launched from single-mode fiber and collimated by a short focal length ball lens, then reflected by a right-angle prism through a window and into the duct. After traversing the duct, the light passes through a window and into a receiving collimator assembly, which focuses light into a 200 um fiber for routing to the detector in the sensor package. Development of this collimator was a major portion of the first Phase of the project.

Since the collimator optics must contend with severe thermal cycling, potential warpage of the scramjet duct and beam steering due to turbulence, the design of the optics was important. The optics must (1) be as tolerant to beam steering as possible; (2) be stable in spite of extreme temperature changes; and (3) be adjustable and lockable for initial alignment when installed in the scramjet duct. Figure 18 sketches the passage of light through a turbulent medium and the parameters to consider (17).
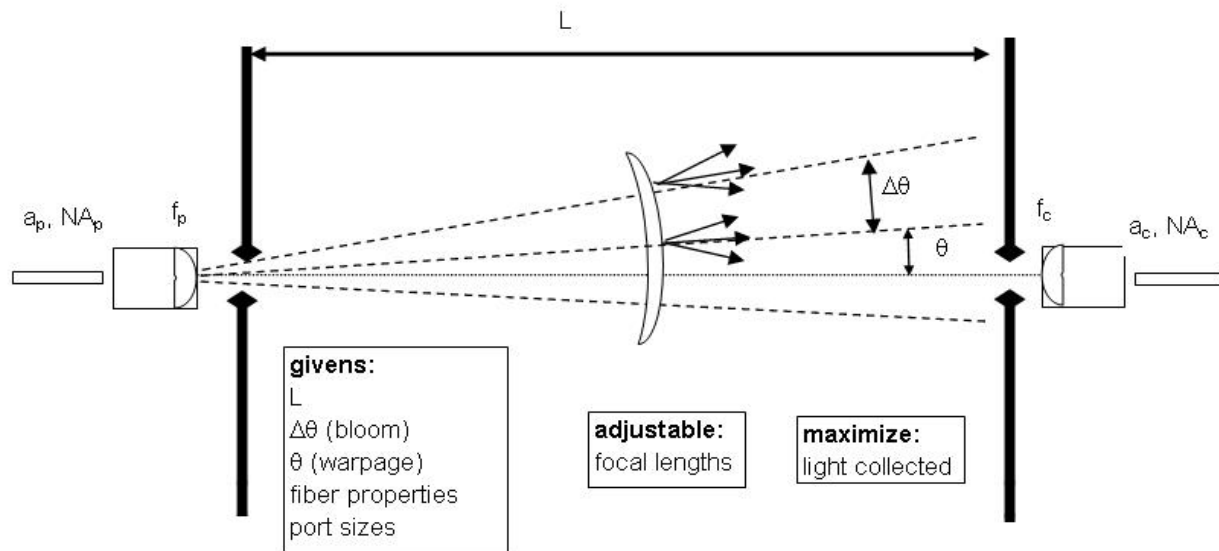
Figure 18: TDLAS send/receive optimization factors

Figure 19 graphs light collection efficiency against catch lens focal length assuming 5 milliradians (0.3 degree) of both beam bloom (due to turbulence) and warpage (due, for example, to thermal expansion). For a given receiving fiber size, there is a trade-off between tolerance to angle and tolerance to lateral shift. Send and receive focal lengths near 5 mm achieve optimal tolerance for fiber cores as small as 50 microns; for optical misalignments less than 5 milliradians, all light incident on the receiving collimator is directed into the receiving fiber; meeting this condition drastically reduces turbulence-induced beamsteering noise.
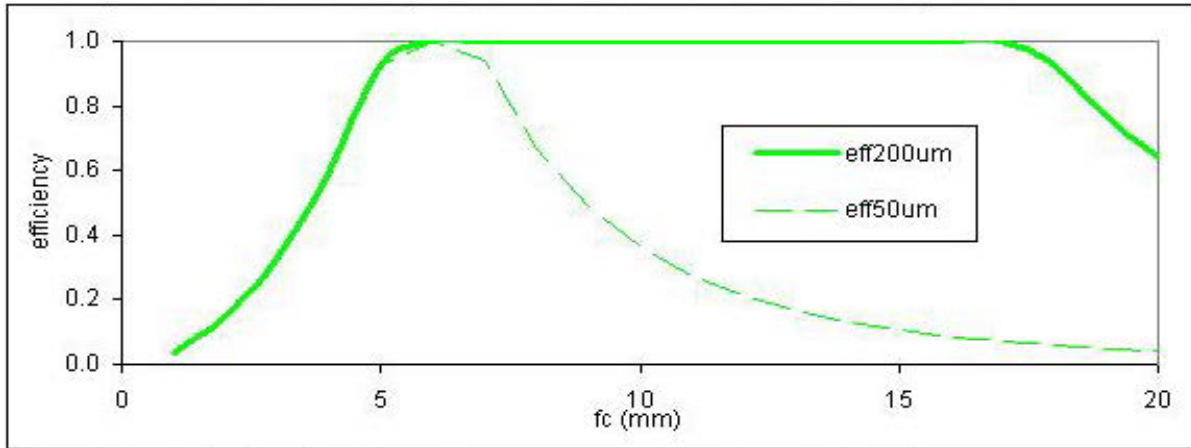
Figure 19: Light collection dependence on receiving optic focal length

Figure 20 depicts the final collimator design. Pitch is set by moving a flexure which tilts the beam-turning prism. Alignment is locked by tightening opposing screws. Yaw is set by rotating the entire collimator and then clamping it into position in a v-groove. This alignment and locking mechanism has been tested to temperatures above 700 K. Figures 21 and 22 show the collimators integrated into a 3 path by 5 path grid in the HIFiRE 2 scramjet duct.
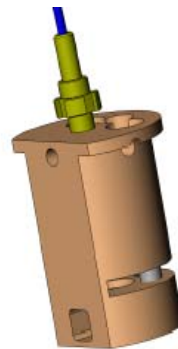
Figure 20: final collimator design
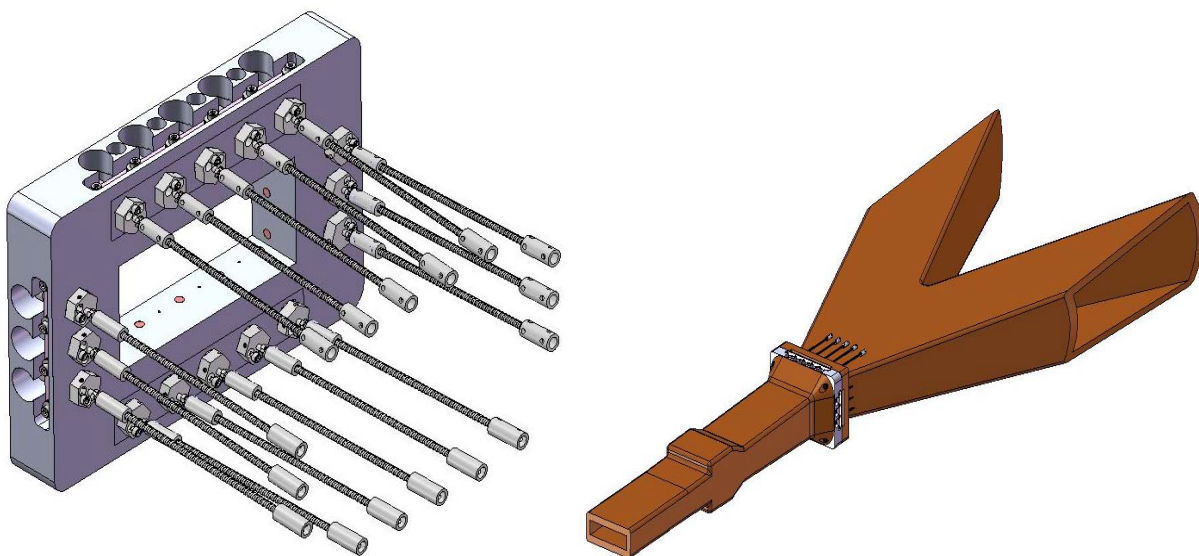
Figure 21, 22: Collimators installed in HIFiRE 2 scramjet duct

7.4 Detectors

New detector assemblies were developed for the Zolo sensor (Figure 23). By using 200 um receiving fibers we make the collimators highly tolerant of misalignment, but the InGaAs detectors are limited to 300 um diameter in order to keep their capacitances low enough for the speed and sensitivity required. Failure to capture all of the light at the detector would lead to excess noise just as at the receiver collimator, and so accurate positioning of the fiber in front of the detector is required.

Figure 23: fiber-coupled detector: 1-assembly body; 2-ferrule mount; 3-ferrule.

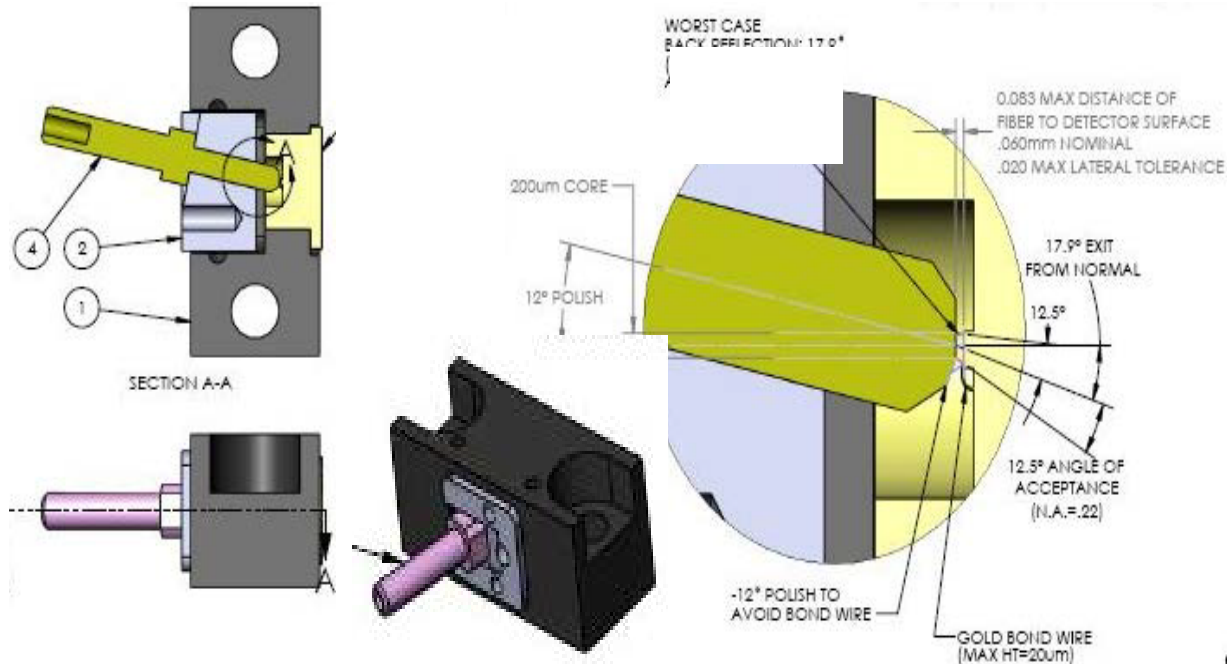Beyond capturing all of the light, the pigtailed detectors must be free of back-reflections that might introduce parasitic etalons. This requires the fibers to be angle-polished and to be brought up to within 170 um of the detector surface at an angle. Finally, the aligned fiber/detector package must be rugged enough to pass NASA's NSROC requirements for vibration and thermal cycling.

7.5 Detector Amplifiers

The transimpedance amplifiers have been optimized for lowest noise with the required bandwidth. To achieve performance beyond what is possible with a traditional single-op-amp design, a topology using two op amps and a FET input was used (18). In order to maximize data output from the sensor package, the analog outputs from the TIAs are buffered and output directly for continuous recording by the sounding rocket's host computer.

Since the sensor must report useful data in spite of varying levels of light transmission, the TIAs have eight gain settings from 10 kilohms to 15 megohms. The system automatically sets the gains to make best use of the ADCs' input range.

7.6 Analog-to-Digital Conversion

In addition to the analog outputs, the detected signals are digitized by four 16-bit, 10-megasample/second analog-to-digital converters (ADCs). Sixteen bits should provide adequate resolution but the signals are ac-coupled and amplified before reading into the ADCs to further minimize bit noise effects. The timing precision must be a small fraction of the sampling time (100 nanoseconds) for effective column averaging.

7.7 Digital Support Circuitry

To handle the 80 megabytes per second of data generated by the four ADCs, processing is accomplished in two phases. A field-programmable gate array (FPGA) performs the column-averaging task, reducing the data rate to a 200-point array updated roughly 7 times per second. This array is transferred to a digital signal processor (DSP) for further computations. Future versions of the Zolo sensor will use the DSP to perform on-board calculation of temperature, concentration and other gas properties, potentially at much higher data rates.

Management of data flow requires a number of clocks and other support circuitry. In addition, the laser driving waveform is generated by a digital-to-analog converter (DAC) outputting a signal generated by the FPGA. Figure 24 shows the flow of data.
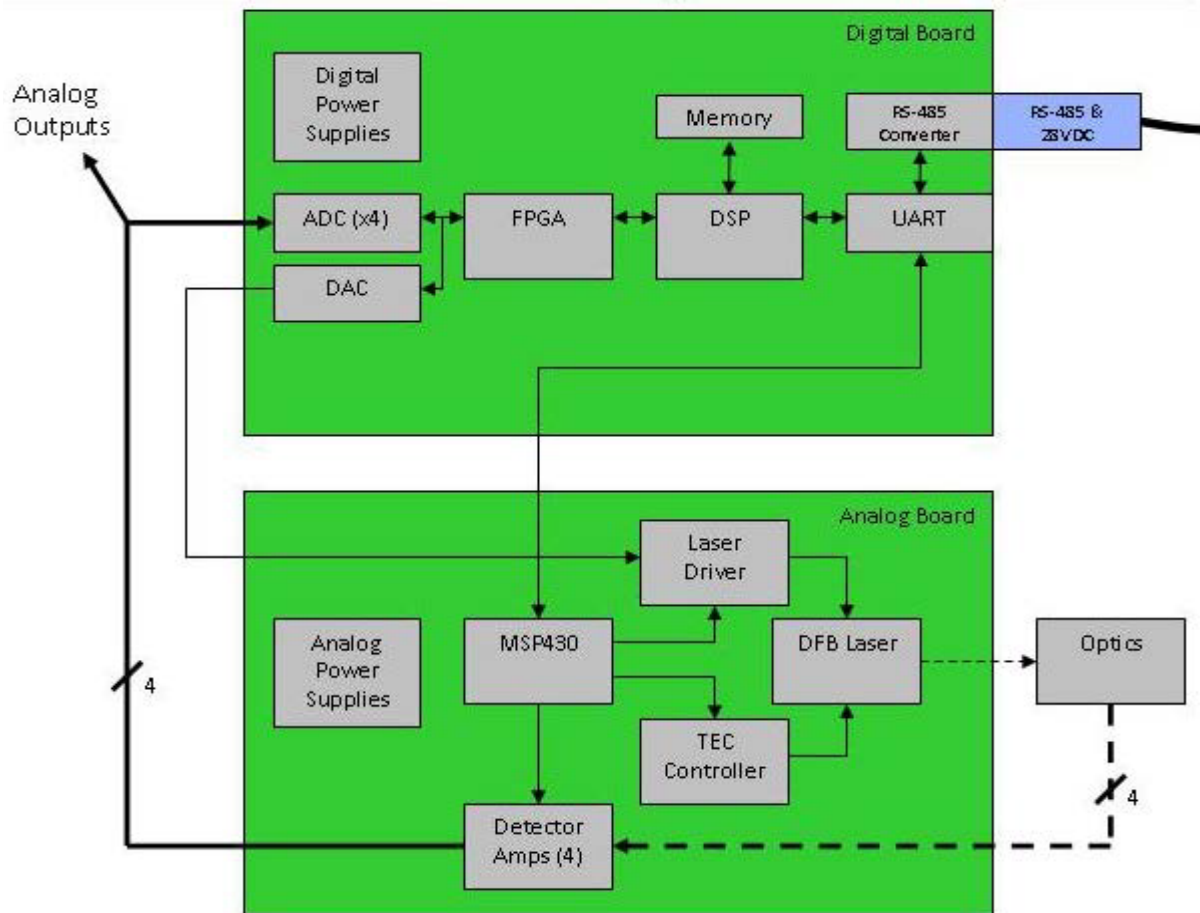
Figure 24: TDLAS sensor data flow

7.8 Electrical Power

The sensor package incorporates power conditioning to use 24-32 Vdc battery power. Total power consumption is typically below 13 Watts.

7.9 Packaging: Thermal/Vibration

The key challenge for the Zolo sensor was to develop a complete sensor package that would survive and function in a sounding rocket. The electronics consume 12 Watts of power which must be managed to avoid overheating; this problem becomes more acute in a compact package. To keep internal temperature rise below 20 degrees C, an overall thermal resistance to ambient air of 1.5 degrees C per Watt had to be maintained; this drove the layout of the PC boards and their heat-sinking inside the package.

More challenging, the sensor package must be free of mechanical resonances up to 2 kHz to survive sounding rocket launch. Zolo's HIFiRE 1 package, based on off-the-shelf electronic assemblies, had numerous internal resonances which vastly amplified stresses on internal components. The new package was designed to minimize internal masses and lever arms and maximize support structure rigidity in order to avoid all internal resonances below 3 kHz. With a rigid and resonance-free structure, internal components need only survive up to the 15-g NSROC specification, which is straightforward for modern telecom and electronic components.

Initial validation of the mechanical design was achieved by careful modeling of the package and all significant components using COSMOS, a finite-element analysis software package. The COSMOS simulation confirmed the absence of mechanical resonances at low frequencies and also provided an estimate of the expected heat rise. By machining the package enclosure out of a single aluminum block containing separate cavities for the analog and digital PC boards, the support structure was made resonance-free and also provided both heat sinking and shielding of electrical noise.

A number of new components were built into the package. They include the distributed-feedback laser, the 1x4 splitter and the custom pigtailed detectors. In addition to the FC/APC connectors used for external fiber connections, the more-compact LC/APC connectors (shown in Figure 25) were used for internal fiber connections. All of these components were subjected to the NSROC test conditions and validated for flight as described below.
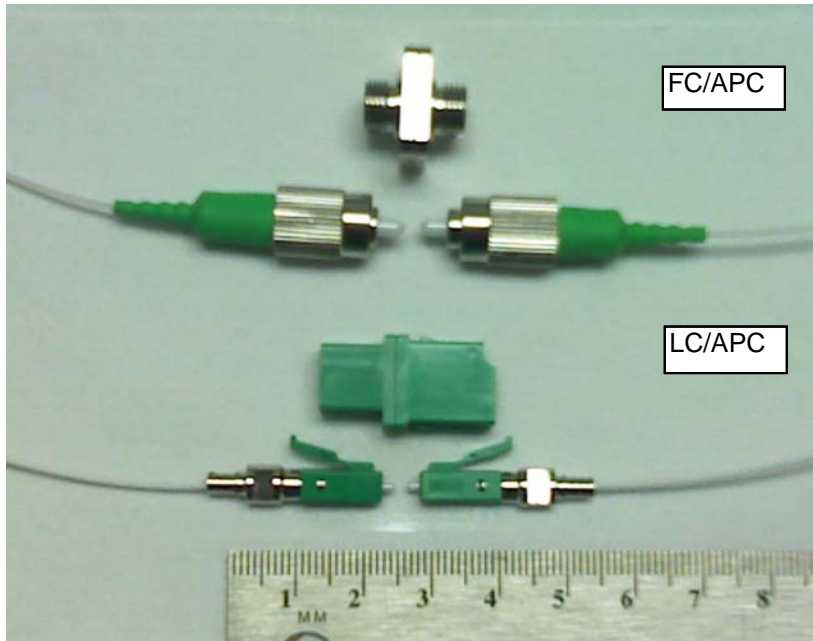
Figure 25: FC/APC and LC/APC fiber connectors

7.10 EMC Considerations

The laser current and temperature and the photodetector currents must be kept free of any noise pickup for proper sensor operation. The noise can come from elsewhere in the host vehicle or may be generated in the noisier digital sections of the control electronics. To ensure signal integrity, the sensitive electronics are confined to the analog PC board while the higher-noise electronics are located on the digital PC board. The sensor case itself is machined from a solid piece of aluminum with separate cavities for the two PC boards. The boards are connected only through two ribbon connectors with appropriate termination of the electrical signals. The detected light signals are amplified and transferred to the digital board as differential signals to maximize noise immunity. After taking these steps, any noise pickup is below our detection level.

7.11 Design for Assembly

While the performance and ruggedness requirements drove the design to be as compact as possible, the practical issue of manufacturability could not be ignored. While electrical connections were limited primarily to two edge-mounted ribbon connectors and connections to the outside world, the fiber connections were more challenging. There were a total of 14 separate fibers to be mounted and two LC fiber connections inside the package (in addition to the 8 FC/APC connections to the outside world). Optical fibers cannot be routed as simply as electrical wires due to fiber fragility and minimum bend radius requirements. Figures 26-28 show the final stages of sensor assembly.
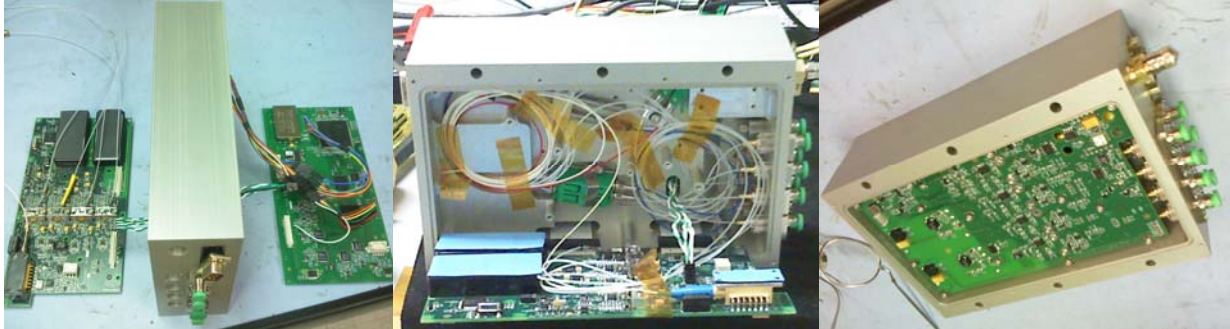
Figures 26-28: sensor assembly

8.0 PERFORMANCE RESULTS

Figure 29 shows absorption spectra generated with 82 milliseconds of averaging. Depicted are low-temperature water absorption peaks at 1350.25 and 1350.42 nm. Three different air paths with lengths of 1.5, 11.0 and 147.3 cm show the data quality for absorption peaks ranging from 0.1% to 25%.
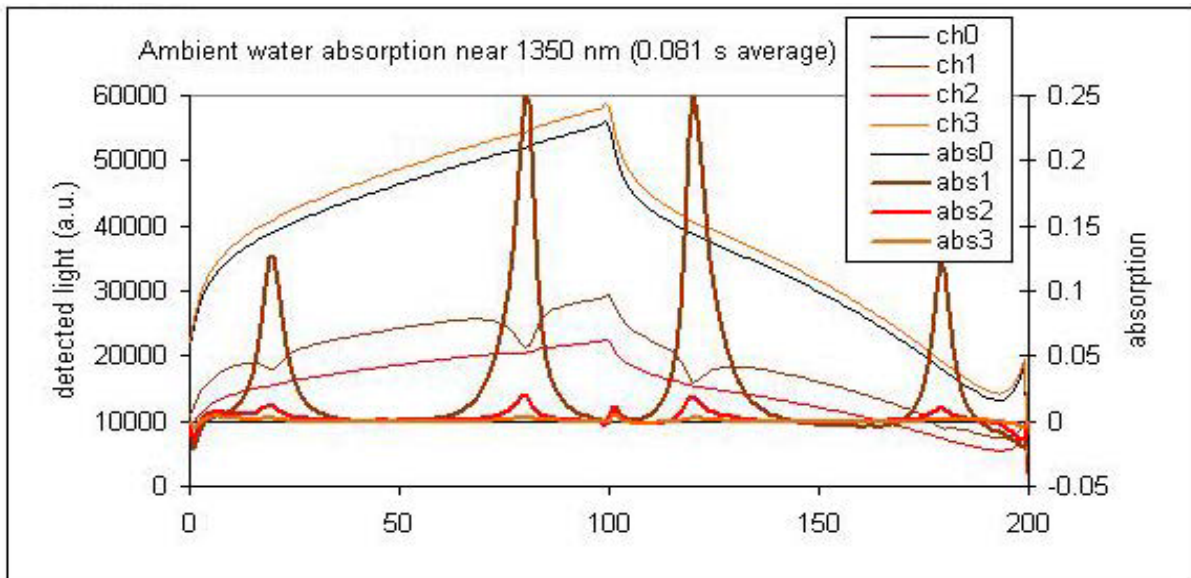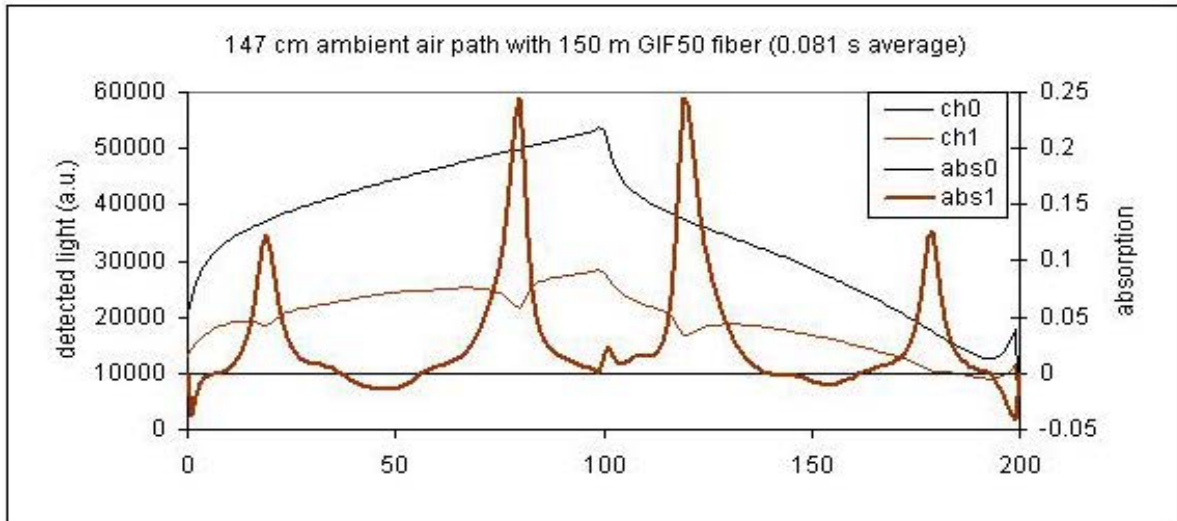

Figure 29: final sensor absorption spectra

We can see the effects of modal noise by placing 150 meters of GIF50 in series with the 147 cm air path (channel 1) as in Figure 30. Ripples appear on the absorption baseline at the few-percent level.

Figure 30: absorption spectrum with 150 meters of multimode fiber

Zooming in on the smaller absorption lines, we can test the immunity to transmission noise. Figure 31 shows how light transmission was varied for channel 3 and Figure 32 shows the resulting spectrum with 0.081 s averaging. This noise level far exceeds what is expected in scramjet duct testing but is typical of light transmission through environments such as coal furnaces. In spite of the transmission noise, the channel 3 spectrum is nearly as quiet as channel 2.
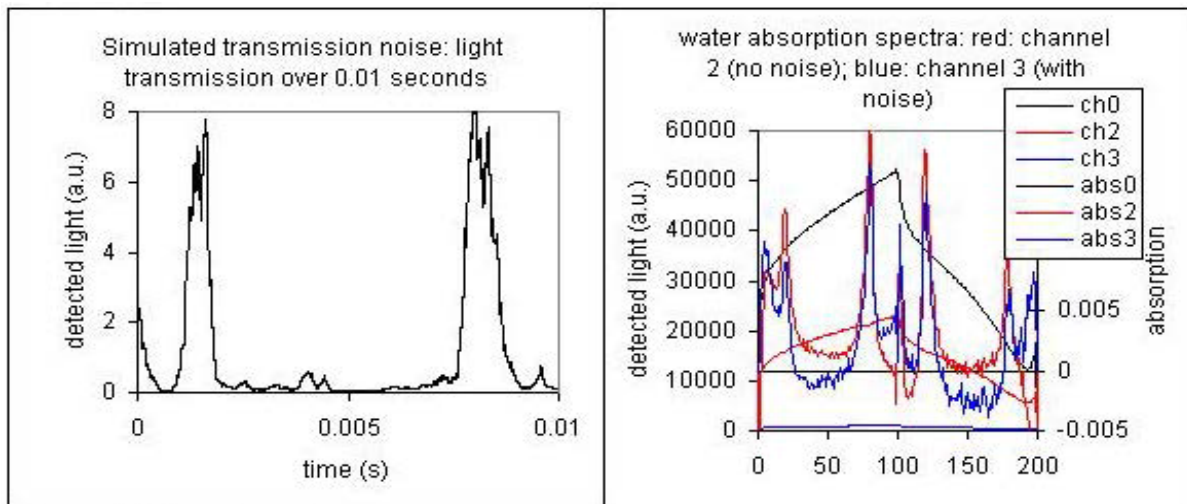
Figure 31: light transmission vs time
Figure 32: absorption spectra with/without transmission noise

The next performance test was to record spectra under low-signal conditions. While initial light transmission across the scramjet duct is expected to be quite high, misalignment or window fouling could reduce light levels severely and the sensor should tolerate this. Figure 33 graphs absorption spectra as detected signal strength is reduced by a factor of 1000. The absorption noise worsens somewhat but the absorption peaks remain recognizable. More significantly, the absorption baseline flatness degrades. This is because the reference waveform was recorded at the lowest detector gain stage while the signal gain was increased as signal strength was reduced. Slight bandwidth and slew rate mismatch between the signal and reference channels led to a distortion of the ratio from which absorption is derived.
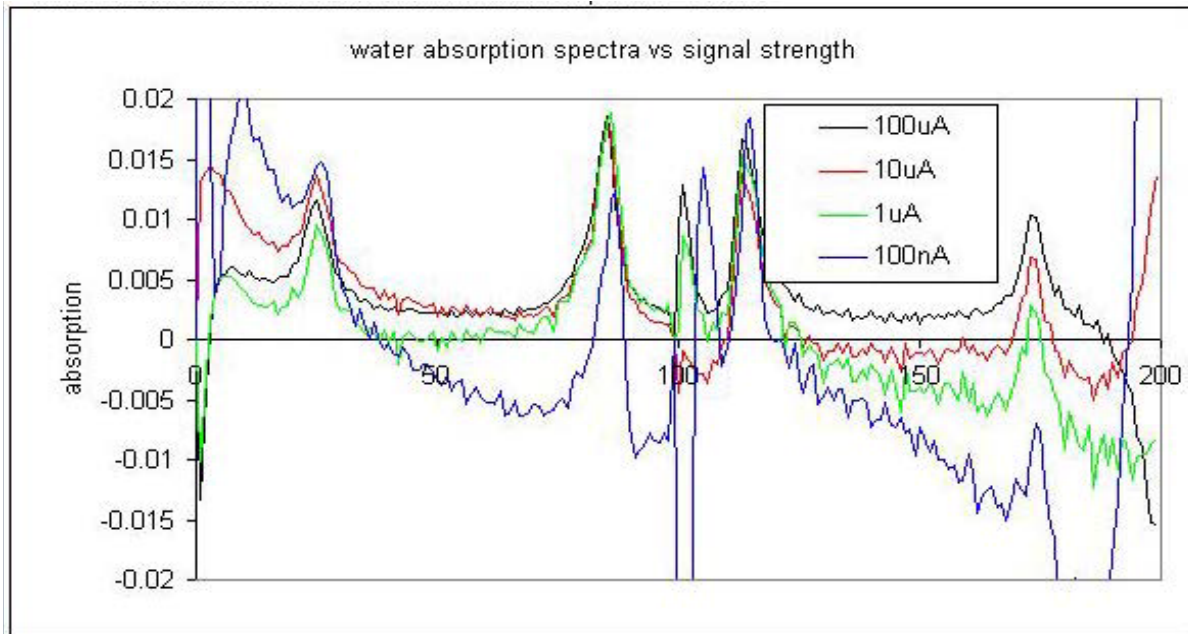
Figure 33: absorption spectra vs detected signal strength

The final performance test took place in the High Impact Technologies Rig facility of the Air Force Research Laboratories at Wright-Patterson Air Force Base. The sensing path was 6 cm long and was immersed in a propane/air flame; in Figure 34 the optical mounting structure for the sensing path is seen glowing white in the lower center of the picture. The high level of turbulence noise anticipated led us to increase the laser scanning frequency to 100 kHz to minimize the effect of the noise on temperature measurement.
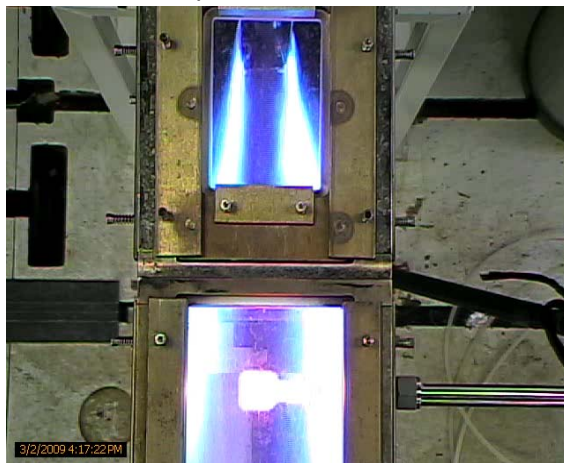
Figure 34: Combustion Test   **Figure 35: 100 absorption spectra**
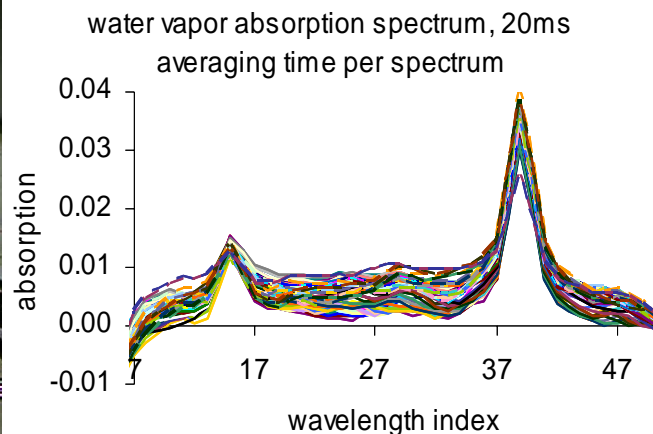
Figure 35 shows a set of 100 sequential absorption spectra collected with 20 milliseconds of averaging (2048 scans) per spectrum. Although peak light absorption is below 4%, the absorption lines remained distinct for all 100 scans. By scanning at 100 kHz, two complete spectra are collected each 10 microseconds, faster than nearly all of the turbulence noise.

The temperature computed from the absorption spectra is seen in Figure 36 along with peak absorption (proportional to the water concentration). An independent temperature monitor with the required temporal resolution was not available to confirm the reality of the observed temperature fluctuations. Further investigation is under way to test sensor sensitivity and accuracy.
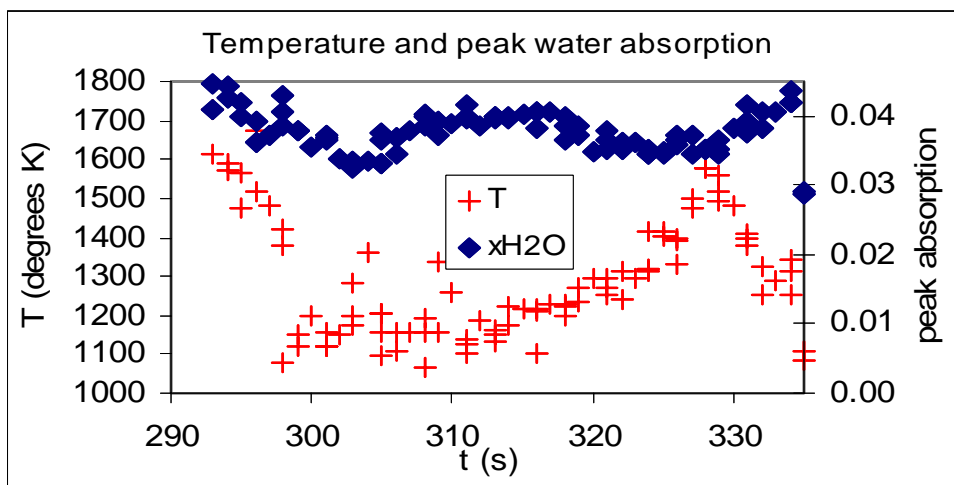
Figure 36: In-flame water concentration and temperature, 20 ms averaging

9.0 FLIGHT QUALIFICATION TESTING

The Zolo sensor was tested to ensure compliance with the NASA NSROC Environmental Testing Policy Manual. As a new component, the sensor underwent the new design qualification testing, intended to expose the test article to conditions beyond those expected in flight. Designing to meet these conditions comprised the bulk of this Phase of the project.

9.1 Thermal Cycling (Operational)

Sensor serial number 2 underwent thermal cycling between 0 C and 61 C to test operational temperature dependence. A total of four cycles with two-hour dwell times at the temperature extremes tested the effects of heating, cooling and thermal soak. To ensure robust start-up, power was cycled at the temperature extremes. As temperature increased, laser wavelength shifted at a rate of 0.8 pm/C for an overall shift of 0.048 nm, as shown in Figure 37. We did not observe any other temperature dependence or any change in performance after thermal cycling.
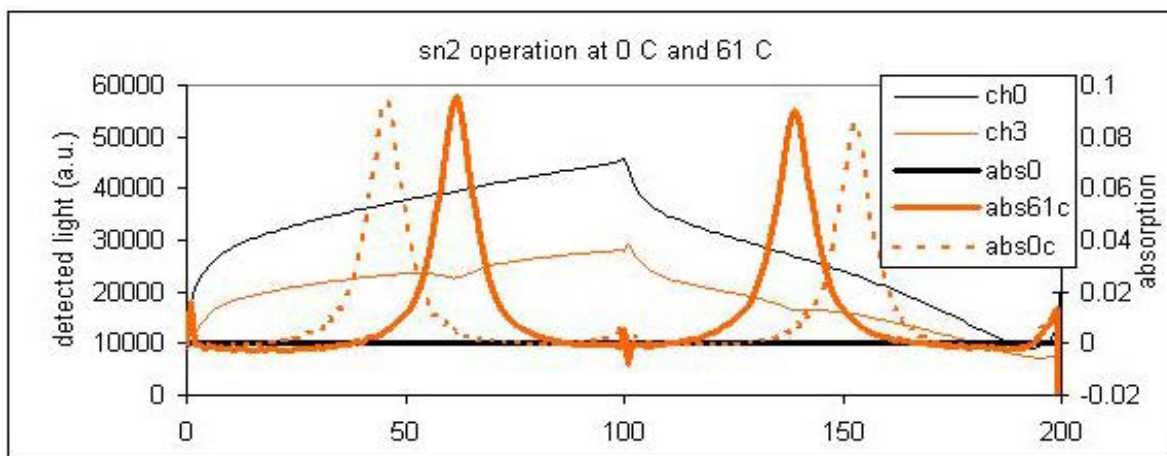
Figure 37: absorption spectra at temperature extremes (no digital control)

The observed wavelength shift was troubling since such a shift during flight might tune one of the two target absorption lines outside of the scanning range and prevent collection of complete spectra. The root cause of the wavelength shift is difficult to discern since many factors combine to set the DFB laser's wavelength. Because of non-zero temperature coefficients of electronic components, the set temperature and set current may drift. As the ambient temperature shifts relative to the laser chip temperature, imperfect isolation of the laser chip from the heat sink temperature will lead to a slight shift of laser temperature away from the control temperature and toward the ambient temperature. Imperfect isolation of the control thermistor or imperfect thermal coupling of the thermistor to the laser chip will also lead to a shift. A shift in the dc level of the scanning waveform input would also result in a current shift and subsequent wavelength shift. Since the electronics were designed with care to minimize these effects, further improvement appeared challenging.

In order to reduce wavelength drift further, we employed a digital control loop. This control loop is based on two observations about the wavelength drift. First, the laser wavelength correlates well with the temperature of the analog PC board, which is monitored with a thermistor built into the microcontroller on the PC board. Second, the thermal mass of the package means that realistic (survivable) temperature changes take place on a time scale of minutes to hours. Therefore a digital re-setting of the laser temperature based on the PC board temperature, applied every 5 seconds, compensates for the observed wavelength shift regardless of its true source. With digital control enabled, we obtained the results shown in Figure 38 and 39:
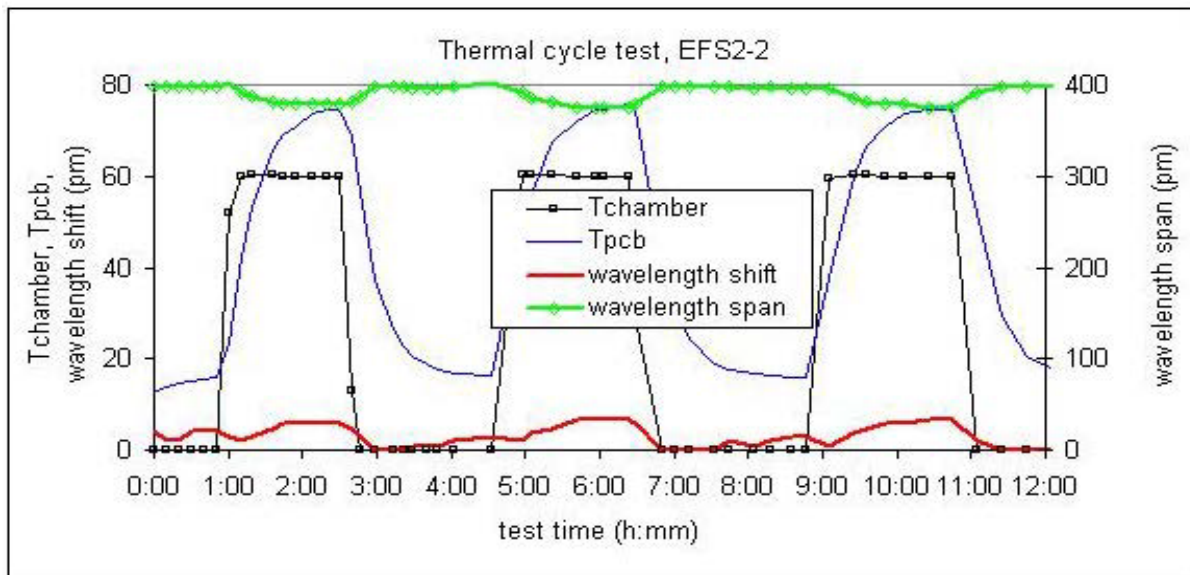
Figure 38: laser wavelength stability with digital temperature control
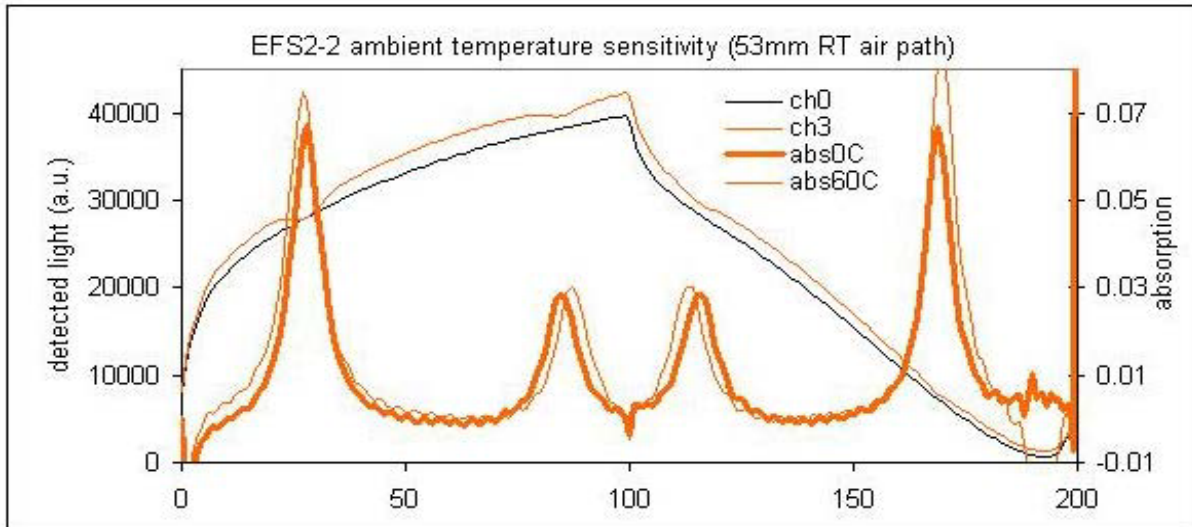
Figure 39: water absorption spectrum with digital temperature control

The overall wavelength shift has been reduced to 0.06 pm/C, or 4 picometers over the 60-degree range. The shift is no longer monotonic; wavelength increases for temperatures above and below 28 C. There is also a small difference in the response to rising and falling temperature. For the TDLAS spectrum, it is now the amplitude of the scanning waveform which shows the dominant temperature dependence. Since the thermal mass of the sensor package should limit any temperature rise during the ten-minute flight to well below the limits tested here, wavelength drift should not be a factor.

9.2 Thermal Cycling (Storage)

For this instrument the NSROC storage temperature requirement was relaxed to a range of -20 C to +85 C. The sensor was held at -20 C for a total of 8.5 hours and at +85 C for a total of 6 hours with one rapid transition from cold to hot and one from hot to cold. Apart from small changes in ambient humidity and a 5% decrease in power (within the margin of fiber flexing), no change in sensor operation was noted (Figure 40).
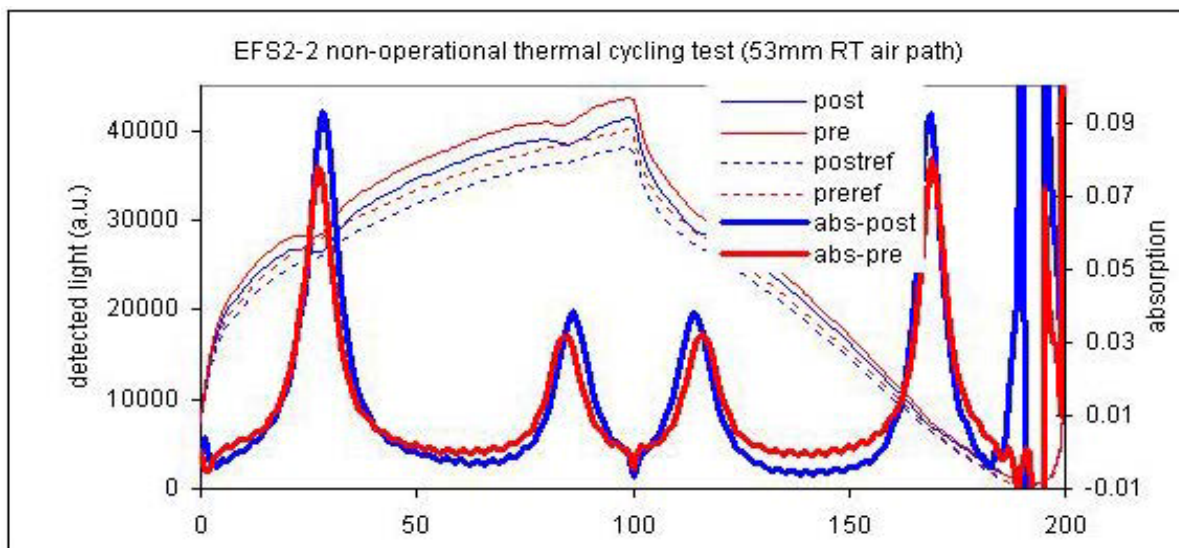
Figure 40: Sensor operation before/after non-operational thermal cycling

9.3 Self Heating

The sensor must operate without heat sinking indefinitely at 61 C. Given 12 Watts of internal power dissipation and 0.078 m^2 in contact with air, we expect internal temperatures to rise about 20 degrees above the ambient air temperature in stagnant air. Since the bulk of the 2.5 kg package is aluminum, the temperature rise should take about 1.6 hours. As Figure 41 shows, in an ambient environment of 70 C we reach an internal temperature of 89.5 C, in accord with expectations. If ambient temperature is limited to 61 C then the internal temperature should not exceed 81 C, which is within the operating range of all internal components.

As noted above, without digital control there is a wavelength shift as package temperature rises due to imperfect control of laser temperature. The total wavelength shift was about 10% of the wavelength scanning range.
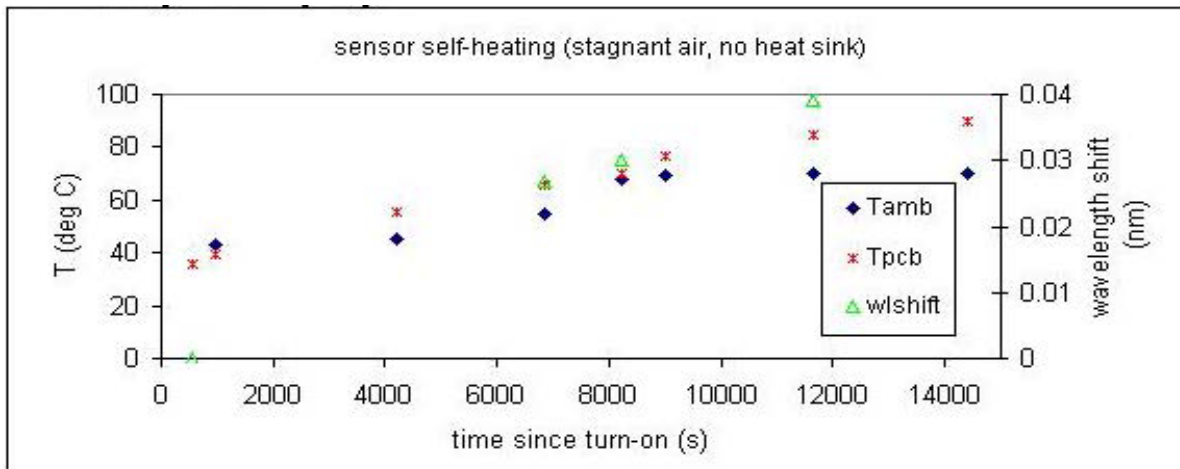
Figure 41: sensor self-heating (no digital temperature control)

9.4 Vacuum

Serial number 1 was subjected to vacuum thermal cycling. While running, the unit was heated to 60 C and then pumped down to a simulated altitude of 109,000 feet (the test chamber's limit). Remaining under vacuum, the unit was cooled to 10 C. Since this experiment was carried out before digital temperature control was implemented, laser wavelength shifted due to the temperature change, but otherwise sensor function and performance remained steady throughout this two-hour test (Figure 42).
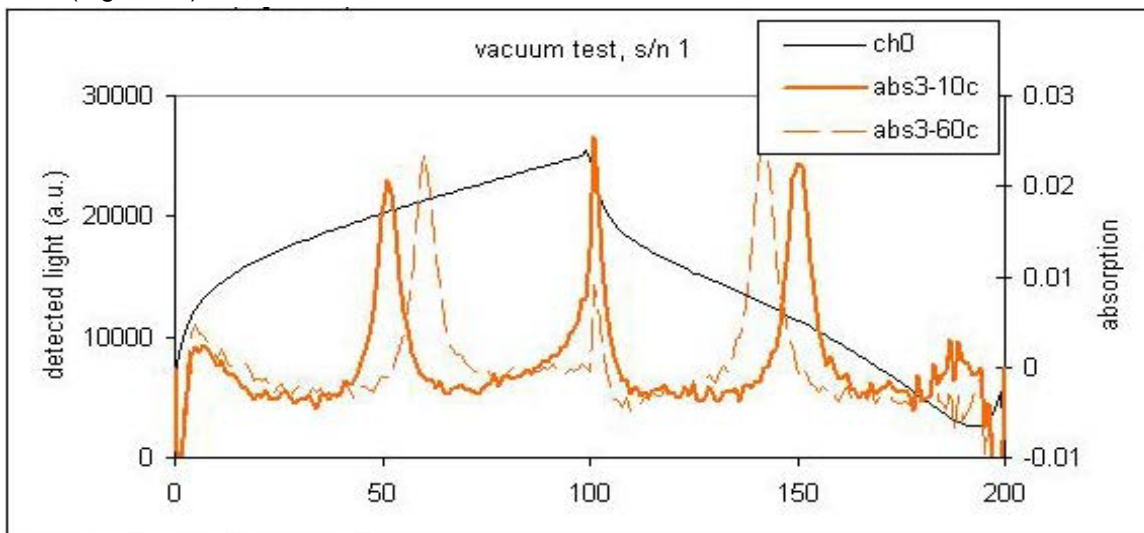
Figure 42: absorption spectra under vacuum (no digital temperature control)

9.5 Vibration

Sinusoidal and random vibration testing was carried out along all three axes. For x and y axes, sinusoidal acceleration was extended beyond the NSROC requirements to 3000 Hz while acceleration was limited to 2500 Hz in the z axis by the test fixture. While the test fixture suffered a modest mechanical resonance near 2500 Hz, sensor performance was unaffected until a few minor mechanical resonances were observed above 2500 Hz. The acceleration testing resulted in no changes in either sensor's performance. Figure 43 shows how absorption spectra changed for serial number 2 over the two-hour test period. Apart from a slight wavelenth drift and changes in electronic offsets with package heating, no performance changes were noted.
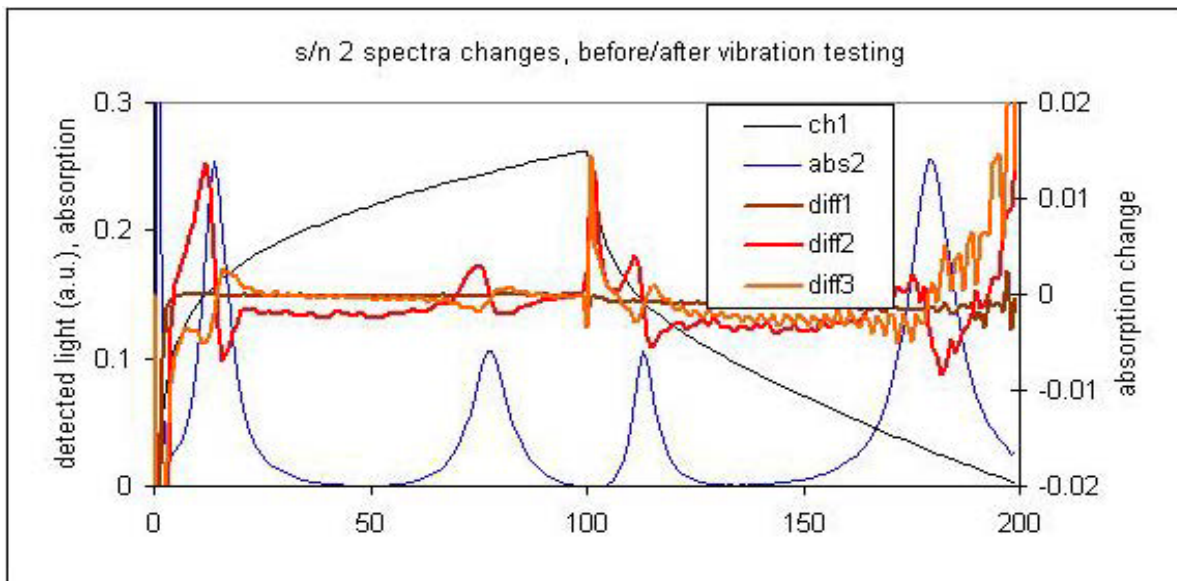
Figure 43: spectral change after vibration testing

Figures 44-47 show average detected signals and raw (un-averaged) spectra collected during sinusoidal and random acceleration.
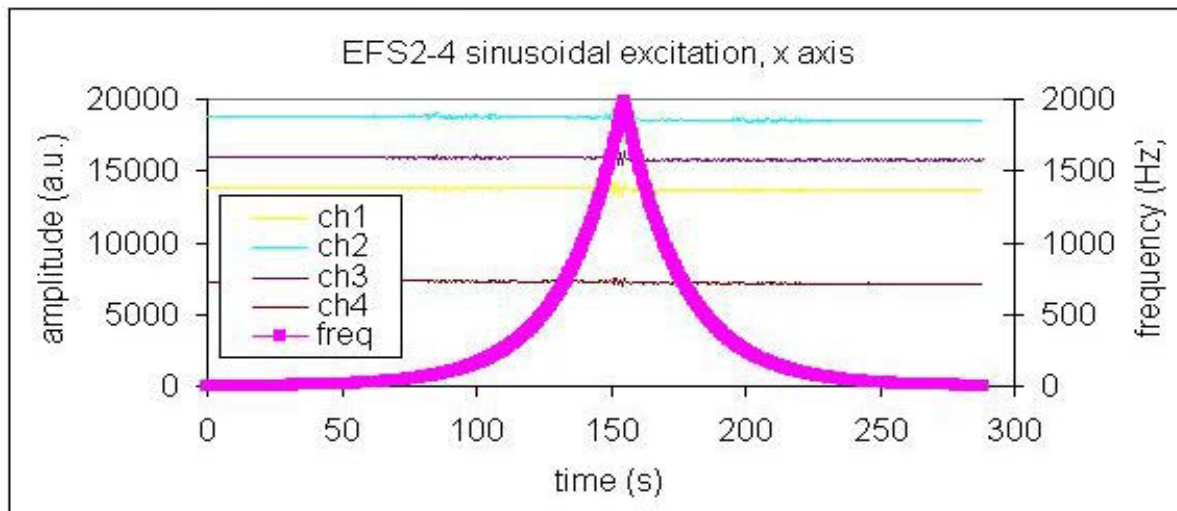
Figure 44: average optical signals during sinusoidal acceleration testing
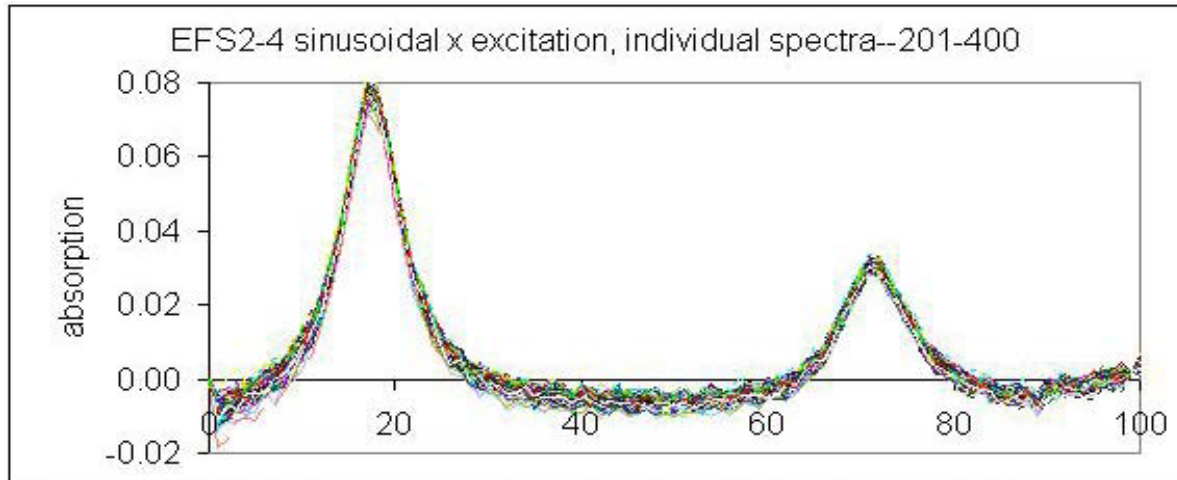
Figure 45: individual absorption spectra during sinusoidal acceleration testing
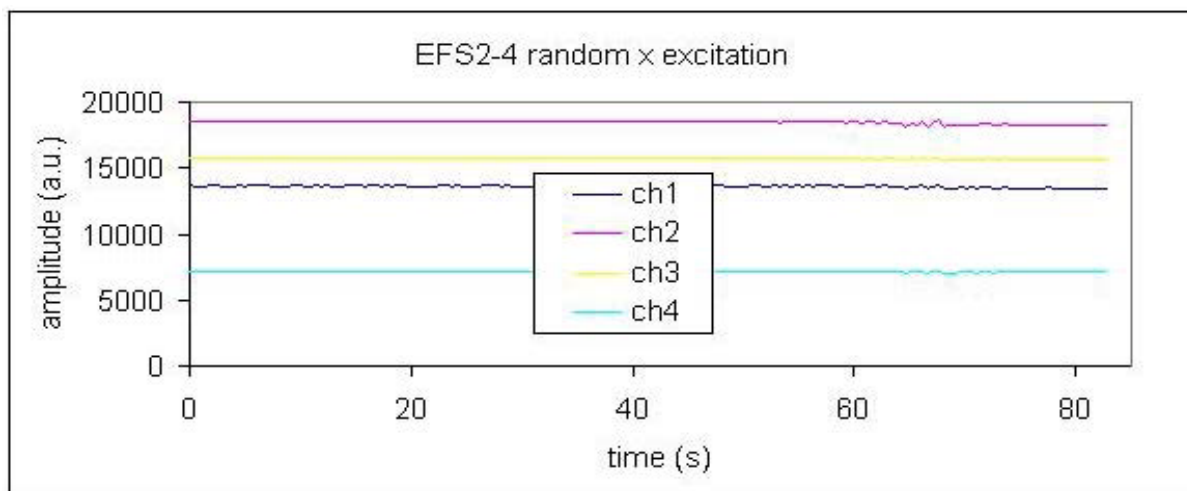
Figure 46: average optical signals during random acceleration testing
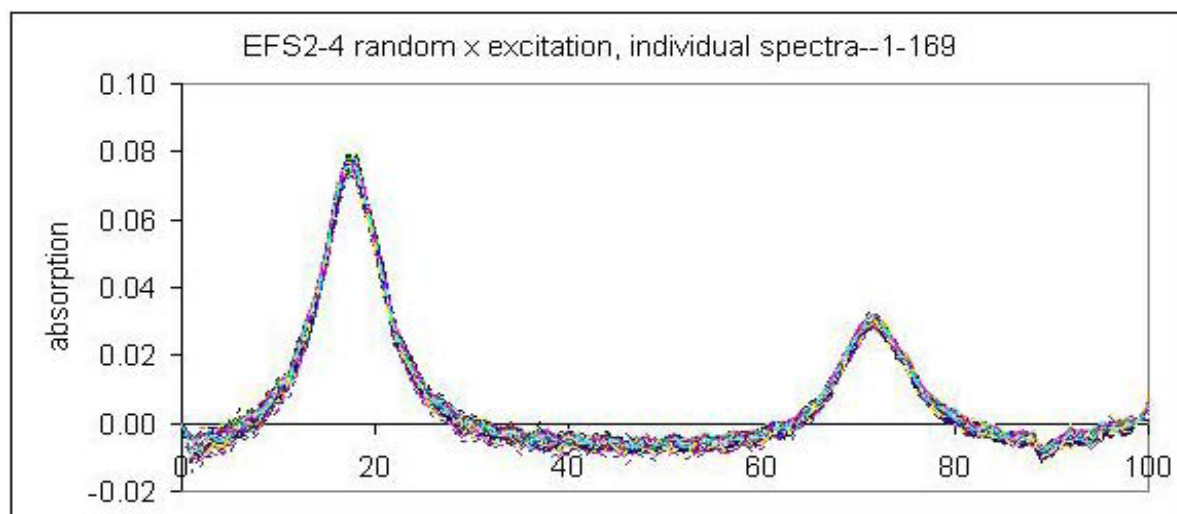
Figure 47: individual absorption spectra during random acceleration testing

An unexpected vibration sensitivity was uncovered on s/n 4 during random acceleration testing. Optical power dropped by a factor of two during the test as shown in Figure 48:
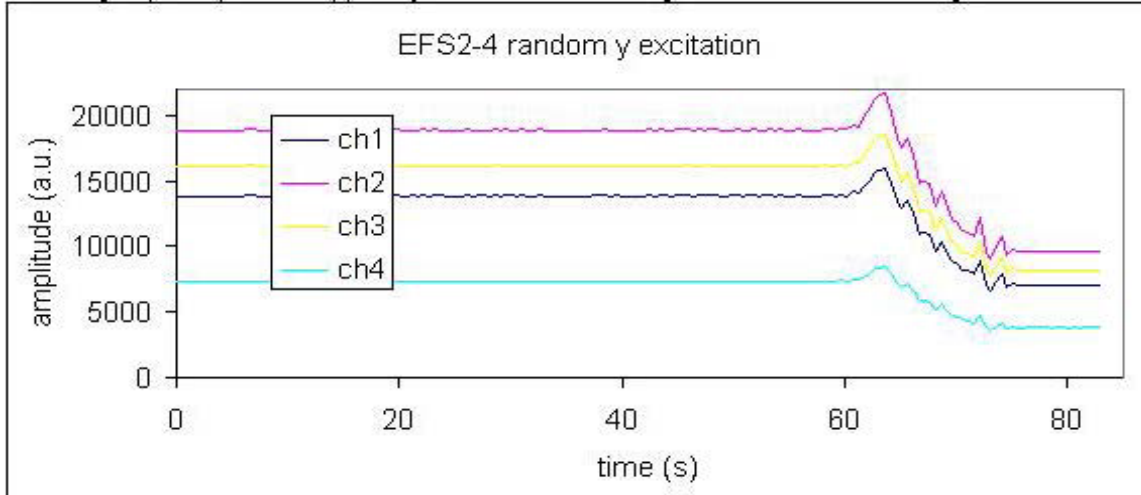
Figure 48: average optical signals during random y-axis acceleration testing

In spite of the drop in power, the recorded absorption spectra remained free of vibration noise:
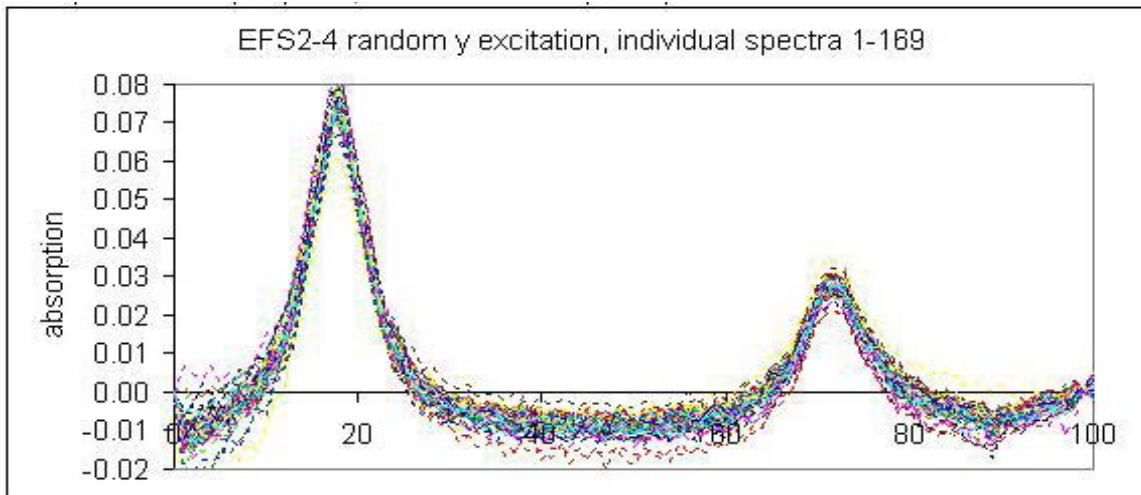
Figure 49: individual absorption spectra during random y acceleration testing

The drop in power was traced to a faulty LC fiber connection between the optical tap and the 1x4 splitter. The latching mechanism of the LC connector failed to latch properly and the LC connectors moved away from each other during vibration testing. This failure mode was corrected and all optical powers returned to pre-test levels. It is important to note that, had this failure occurred in flight, the recorded absorption spectra would have remained of high enough quality to compute temperature and other quantities. In order to degrade the recorded absorption spectra, a power loss greater than 99% would be required.

By passing the NSROC vibration specifications, we can confirm the flight-worthiness of a number of components. The DFB lasers' performance was unaffected by the acceleration tests. Both the 2x2 attenuator and the 1x4 splitter also performed without problems; this is a distinct improvement over the fiber coupler performance observed during the first Phase of this project, when package mechanical resonances led to severe optical noise generated in the couplers. We also observed no problems with the FC connectors or with the custom-built fiber-coupled detectors. Of the 8 LC connections undergoing acceleration testing, we observed the one failure discussed above.

9.6 Shock and Acceleration

The sensor has been designed to withstand the 60-g launch acceleration with an acceptable safety margin. Acceleration tests have not been conducted but will take place as part of payload integration.

9.7 Power Supply Voltage

Figures 50 and 51 show operation over the specified power supply range of 24 to 32 V dc. Sensor operation was within expected limits over this range.
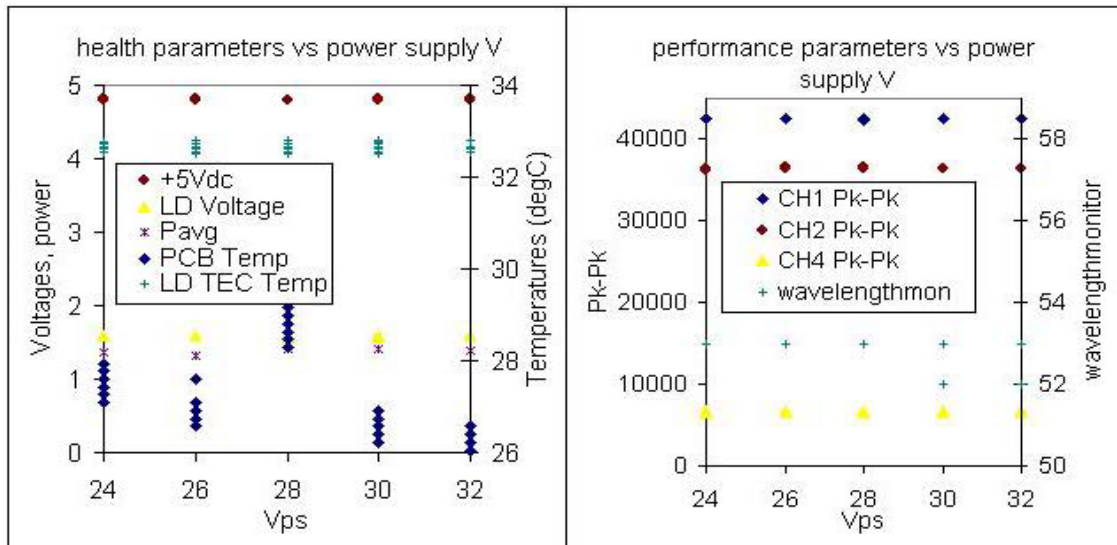
Figures 50, 51: sensor operation vs power supply voltage

9.8 Power Supply Current Inrush

Figure 52 shows the sensor current draw at turn-on. There is a large spike upon turn-on as the digital electronics are energized. The sensor contains slow-blow fuses to tolerate this spike but it is important to know the current inrush characteristics since the battery power supply in the sounding rocket will supply is capable of supplying a very high current.
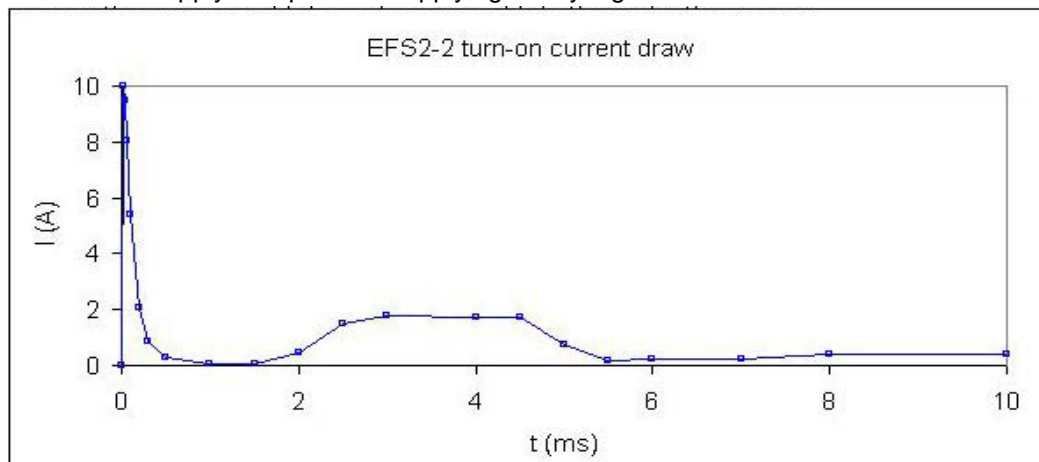
Figure 52: power supply current in-rush at turn-on

conclusion

The NSROC test results demonstrate the flight-worthiness of the Zolo sensor for HIFiRE flights. Appendix B lists the specifications for the sensor package.

10.0 PERFORMANCE EXPECTATION FOR HIFiRE FLIGHT 2

The sensor described here was designed for the TDLAS experiment to be carried out in the Fall of 2010 on the second flight of the Hypersonic International Flight Research Experimentation (HIFiRE) Program, a collaboration between the US Air Force Research Laboratory (AFRL), NASA and the Defence and Science Technology Organisation (DSTO). References 20 and 21 describe HIFiRE Flight 2 in detail. The primary objective of the flight is to evaluate hydrocarbon-fueled scramjet performance over the transition from dual-mode to scramjet operation near Mach 5.5 up to full scramjet operation near Mach 8. This affords the opportunity to perform TDLAS measurements over this extended flight envelope. Figure 53 shows the complete sounding rocket and the payload section.
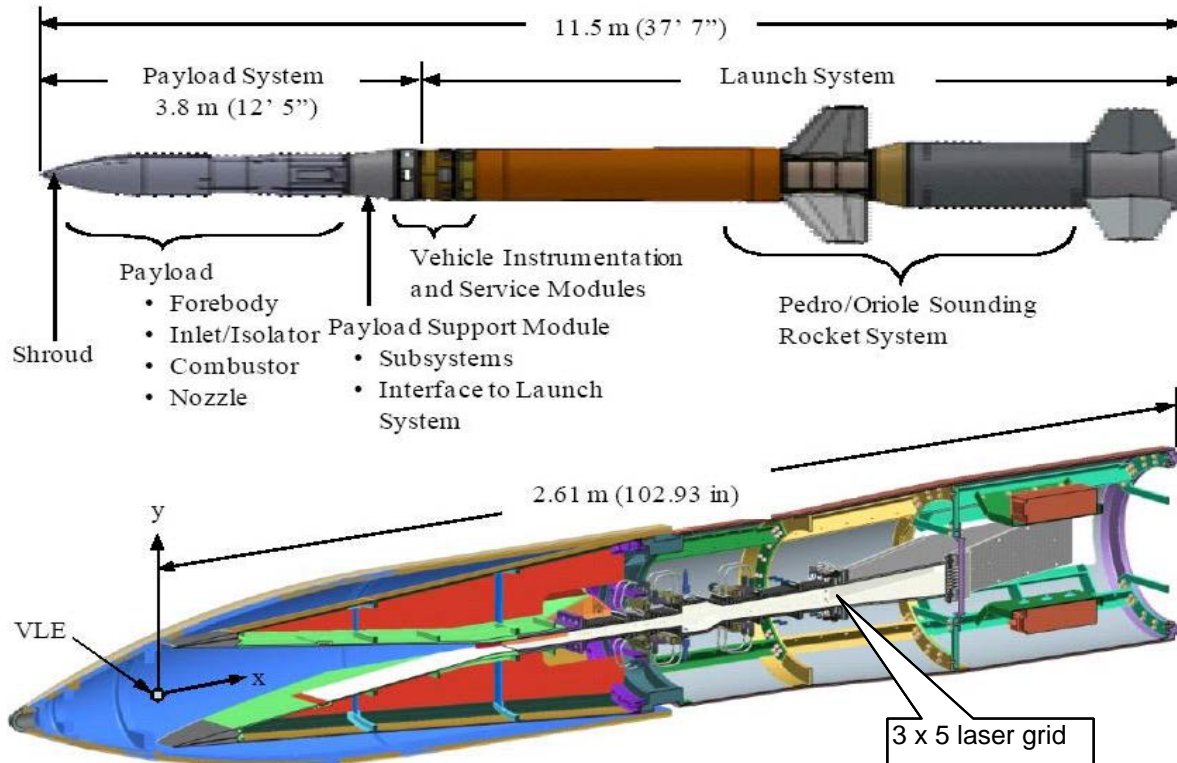
Figure 53: HIFiRE Flight 2.

A 3 x 5 grid of laser paths are situated immediately in front of the bifurcated exhaust nozzle section as indicated. Table 3 of Reference 21 summarizes the expected conditions:

fuel: 64% ethylene, 36% methane (surrogate for cracked JP-7 fuel)
vehicle speed: Mach 6 to 8
exhaust static pressure: 2.0 - 3.0 atm
exhaust temperature: 1560 - 2531 K
exhaust gas composition: 72.2% N_2, 14.8% H_2O, 12.0% CO_2, 0.9% Ar (for ideal, stoichiometric combustion)
gas path lengths: 48.5 mm (short paths), 101.6 mm (long paths)

Assuming a 20-millisecond averaging time (1000 scan averages), we can estimate the temperature and concentration measurement uncertainties. Figure 54 graphs these uncertainties over the range of expected temperatures.
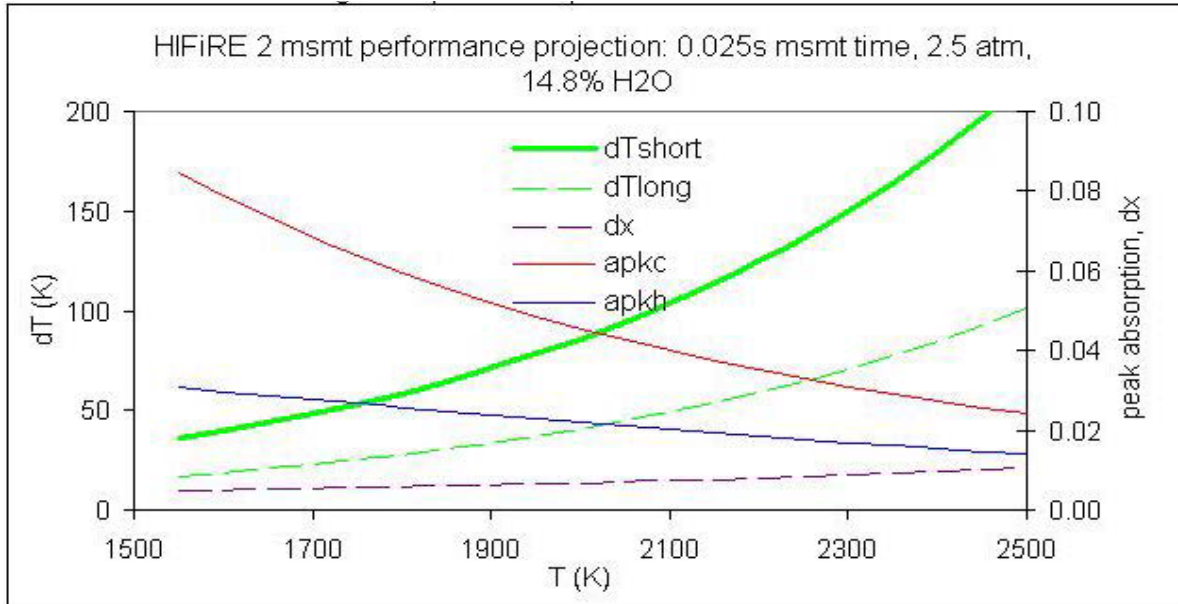
Figure 54: HIFiRE Flight 2 TDLAS measurement performance projection

The temperature measurement uncertainty for the short paths is shown in solid green and for the long paths in dashed green. The peak absorptions for both key absorption lines (in red and blue) remain below 10% throughout the 1500-2500 K range. The nominal temperature uncertainty near 100 K amounts to a 5% relative measurement uncertainty. The water concentration uncertainty (dashed purple) stays below 1% over the expected temperature range.

Since Figure 54 shows the expected performance with ideal, stoichiometric combustion, this is the best measurement performance we expect. Temperature and concentration uncertainty will be degraded during scramjet engine start-up and as the fueling is ramped down toward lean blow-out after conclusion of the experiment period. Since the TDLAS sensor will record and transmit data throughout the flight, the sensor's peformance across a range of conditions will be tested.

In addition to the TDLAS sensor, the HIFiRE 2 payload contains more than 100 pressure sensors and numerous wall temperature sensors. The direct but non-intrusive measurement of gas conditions enabled by TDLAS provides a new window into combustion performance that should be a valuable complement to existing temperature and pressure sensors.

11.0 FURTHER DEVELOPMENT

The sensor described here can be modified to measure other quantities of interest. By extending the wavelength scanning range or combining two packages with different laser wavelengths, complex spectra can be recorded to derive spatially-resolved temperature and concentration (14). By using the Doppler effect, flow field velocity and, hence, mass flux can be determined (15). Using different laser wavelengths, other species of interest such as oxygen, carbon dioxide and carbon monoxide may be sensed. The fluctuations of light transmitted through the target medium can yield information on flow field turbulence and instabilities.

Beyond advanced hypersonic vehicles, the energy and transportation requirements of civilization depend on burning hydrocarbon fuels, and this will not change for several more decades. TDLAS sensor information can lead to cleaner, more efficient combustion; in general, more power delivered for less fuel burned, less pollution and less waste heat. Zolo intends to apply the technologies described here in coal power plants, gas and steam turbines, incinerators and other power-generating systems.

12.0 REFERENCES

1 Craig Covault, "The HiFire Flight Tests Will Help Integrate Aeronautics and Space Technologies," Aviation Week, March 18, 2007.
2 G B Rieker et al, "A diode laser sensor for rapid, sensitive measurements of gas temperature and water vapour concentration at high temperatures and pressures", Measurement Science and Technology, 18 (2007), 1195-1204.
3 L. S. Rothman et al, J. Quantum Spectrosc. Radiat. Transf. 96 (2005), 139.
4 R. J. Barber et al, Monthly Notices of the Royal Astronomical Society 368 (2006), 1087.
5 Miniaturized Laser-Based Measurement Capability Aids Scramjet Engine Performance Analysis, AFRL SBIR/STTR Technology Milestones 8/11/2006.
6 GB Rieker, H Li, X Liu, JB Jeffries, RK Hanson, MG Allen, SD Wehe, PA Mulhall, HS Kindle, "A diode laser sensor for rapid, sensitive measurements of gas temperature and water vapor concentration at high temperatures and pressures ," *Measurement Science and Technology* **18** , 1195-1204 (2007).
7 M. B. Frisch et al, "Progress in reducing size and cost of trace gas analyzers based on Tunable Diode Laser Absorption Spectroscopy", SPIE Optics East Advanced Environmental, Chemical and Biological Sensing Technologies II (Philadelphia, PA) 26 October, 2004
8 M. G. Allen et al, "Overview of Diode Laser Measurements in Large-Scale Test Facilities", AIAA-2000-2452, 21st Aerodynamic Measurement Technology and Ground Testing Conference, 19-22 June 2000 (Denver, CO).
9 X Zhou, Ph.D. Dissertation, Stanford University, July 2005.
10
   "*Frequency Modulation Spectroscopy for Trace Species Detection: Theory and Comparison Among Experimental Methods* ," J. A. Silver, Appl. Opt. **31**, 707 (1992).
11 "*Frequency Modulation and Wavelength Modulation Spectroscopies: Comparison of Experimental Methods Using a Lead-Salt Diode Laser* ," D. S. Bomse, A. C. Stanton and J. A. Silver, Appl. Opt. **31**, 718 (1992).
12 G. B. Rieker et al, "Measurements of near-IR water vapor absorption at high pressure and temperature", Applied Physics B 87(2007), 169-178.
13
   P. C. D. Hobbs, "Ultrasensitive laser measurements without tears", Applied Optics 36 (1997), 903.
14 Jun Ye et al, "Ultrasensitive detections in atomic and molecular physics: demonstration in molecular overtone spectroscopy", J. Opt. Soc. Am. B 15 (1998), 6.
15 Chad Lindstrom et al, "Diode laser absorption tomography using data compression techniques", In press, 2008.
16 B.L. Upschulte, M.F. Miller, M.G. Allen, K. Jackson, M. Gruber, T. Mathur, "Continuous Water Vapor Mass Flux and Temperature Measurements in a Model SCRAMJET Combustor Using a Diode Laser Sensor," AIAA Paper 99-0518, presented at 37th AIAA Aerospace Sciences Meeting and Exhibit (Reno, NV), , (11-14 January 1999).
17 L. A. Kranendonk and S. T. Sanders, "Optical design in beam steering environments with emphasis on laser transmission measurements," *Appl. Opt.,* vol. 44, pp. 6762-6772, 2005.
18 G. Brisebois, "LT1806: 325MHz Low Noise Rail-to-Rail SOT-23 Op Amp Saves Board Space", Linear Technology Design Note 254, 2001.
19 J. Howell, Zolo internal memo, March 2003.
20 Kevin R. Jackson, Mark R. Gruber, and Todd F. Barhorst, "The HIFiRE Flight 2 Experiment: An Overview and Status Update", AIAA-2009-5029, 45th AIAA/ASME/SAE/ASEE Joint Propulsion Conference, 2-5 August 2009, Denver, Colorado.
21 Mark R. Gruber et al, "Instrumentation and Performance Analysis Plans for the HIFiRE Flight 2 Experiment", AIAA-2009-5032, 45th AIAA/ASME/SAE/ASEE Joint Propulsion Conference, 2-5 August 2009, Denver, Colorado.

APPENDIX A: TDLAS SIGNAL PROCESSING

THE ESSENTIAL GOAL OF THE ZOLO EMBEDDED FLIGHT SENSOR

The purpose of Zolo's products is determination of laser light absorption due to target molecules along a path through a harsh environment. We expect a great deal of light absorption not due to our target molecules, and we expect additional light not from our lasers to confuse the issue. The unwanted light absorption and background light are expected to be wildly varying, and both may be far greater in magnitude than the absorption signal we seek to measure.

Regardless of the gas to be detected, the TDLAS sensor should achieve the following:

1. Measure absorptions from tens of percent to tenths of percent or less.

2. Perform stable measurement in the face of large and fast transmission fluctuations. The maximum fluctuation rate can be hundreds of kilohertz (or even faster for high-performance aircraft turbines), typically following a 1/f power spectrum.

3. Measure with a rapid update rate (perhaps a thousand measurements per second in aeropropulsion applications).

These three requirements may be combined into a single figure of merit for comparing different measurement strategies:

$$\text{FOM} = [(\text{minimum detectable absorption dip}) \times (\text{measurement time})^{1/2}] / (\text{noise})$$

Implicit in the first requirement is measurement stability or robustness: a consistent absorption value must be returned for a constant gas density and temperature, in the face of all other disturbances.

To be able to measure the smallest absorptions, we must account for all factors that can affect the detected light level and might be confused with molecular absorption. In this Appendix we describe the detected light signals and how we process to derive clean absorption spectra.

DEFINITION OF QUANTITIES IN THE ZOLO TDLAS SENSOR (18)

For each laser wavelength range or channel i, two streams of data are collected. The first, or reference, is proportional to the light power emitted by the laser:

$$I_{Ri}(\nu) = r_i P_{Li}(\nu) \exp[-m_r(\nu)]$$

where $P_{Li}(\nu)$ is the laser's output power. The frequency $\nu = \nu(t)$ is now scanned up and down in a quasi-triangle waveform with a repetition rate of 2-200 kHz, and the laser power increases and decreases as the wavelength changes. The reference signal is measured with negligible detector noise and offset. The reference signal may have modal noise m_r but the magnitude is also generally negligible.

The second data stream is the power that is transmitted through the gas and subsequently detected:

$$I_{Si}(\nu) = \{D_i(t) + b_i B(t)\} + \beta(\nu,t) P_{Li}(\nu) T_{gasi}(\nu)$$

where

$D_i(t)$ = photodetector noise (random white noise up to the detector bandwidth limit); $\langle D_i \rangle = 0$

$B(t)$ = emission background light; $\langle b_i B(t) \rangle = b_i B_0$, $B(t)$ may fluctuate by a factor of 2 on time scales that are typically much longer than the TDLAS wavelength scan time. (Apart from a constant scale factor b_i accounting for detector responsivity, the background tends to be well-correlated among different multiplexed laser channels.)

$\beta(\nu,t) = t_i T_{fb}(t) T_{MNi}(\nu)$ = multiplicative noise (due to laser amplitude noise and transmission noise)

The multiplicative noise may be broken down further:

$$T_{fb}(t) = \beta_0(t) [1 + n_m(t)]$$

where $\beta_0(t)$ is a slow but widely-varying function between 0 and 1 due to slow transmission fluctuations (for example, vibration-induced beam-steering) while $n_m(t)$ accounts for faster and smaller transmission noise (typically 1/f in character).

$T_{MNi}(\nu)$ = systematic multiplicative noise = $\exp[-m_s(\nu)] = 1 - \Sigma[c_q \sin(q\,k\,\nu + \phi_q)]$, $|c_q| \ll 1$

Etalon ripples and modal noise are included in this term, which is not improved by averaging.
Finally, the signal of interest is contained in the final factor:

$T_{gasi}(\nu) = \exp[-\alpha_{toti}]$

Assuming a uniform path, the absorption is:

$\alpha_{toti} = P\,L\,\{x\,\Sigma\,S_j(T)\,g_j(\nu, T, P) + f_{inti}(\nu)\,\}$

where
P = pressure
L = path length
x = target gas concentration
$S_{ij}(T)$ = absorption line strength of jth line for ith laser

$g_{ij}(\nu)$ = normalized absorption line shape vs wavelength $(\int g(\nu)\,d\nu = 1)$

$f_{int}(\nu) = a + b\nu + c\nu^2$ is a quadratic fit to the absorption of nearby interfering lines (or a fit to modal noise)

It is the concentration x that is the quantity to be measured. If noise and background are low, then this can be done to a precision limited by interfering absorption lines.

COLUMN-AVERAGED PHOTOCURRENT SIGNALS

We average over many scans (2048 for the HIFiRE 2 sensor) to reduce the random noise sources. This leaves us with the following:

$<I_{Ri}(\nu)> = R_i(\nu) = r_i\,P_{Li}(\nu)\,\exp[-m_r(\nu)]$

$<I_{Si}(\nu)> = b_i\,B_0 + t_i\,\beta_0\,T_{MNi}(\nu)\,P_{Li}(\nu)\,T_{gasi}(\nu)$

We assume that we have an estimate for the background term $b_i\,B_0$ which differs from the actual background by a (presumably small) term Δ. Subtracting off the background, we can then take the log-ratio and generate the absorption spectrum (henceforth we drop the subscript i and focus on one laser channel at a time):

$A(\nu) = -\ln[(I_S - b\,B_0)/I_R] = \ln[r/(t\,\beta_0)] + \alpha_{tot}(\nu) + (m_s(\nu) - m_r(\nu)) + \{\Delta/[t\,\beta_0\,P_L(\nu)]\}\,\exp(\alpha_{tot}(\nu) + m_s(\nu))$

This function in "absorption space" is the most important to us and easiest to evaluate since we have divided out the details of laser power modulation and light transmission. Examination of this function tells us our measurement quality fairly directly.
--The first term is a constant, independent of frequency, and is of no concern (except possibly as a monitor of light transmission).
--The second term is what we wish to determine.
--The third term is the modal and etalon noise from both the signal and reference. In wavelength space this term is a sum of sinusoids of random phase, amplitude and frequency, changing constantly as launch conditions and fiber state change. Fortunately, it can be made quite small (<0.1%) if fiber lengths are kept below about 50 meters.

--The final term is due to our imperfect removal of background light. Since background light may be far greater than the detected laser light in some combustion situations, this term is potentially a problem. If our wavelength scan range is large enough so that we can scan to where the target absorption α_{tot} is small then the background light can be calculated accurately enough that its effect on the absorption spectrum is comparable to that of modal noise; this is generally good enough.

CONTROL OF SYSTEMATIC AND PROCESSING ERRORS
The raw signals S and R are distorted by various artifacts which have different symmetries and different systematic behaviors. Table A-1 lists the artifacts that often afflict TDLAS measurements. By using a triangle scanning waveform, we can identify artifacts by their symmetries. The following points are of note:
1. Backgrounds and offsets: the combination of a non-zero background (or detector or A/D offset) and the laser amplitude modulation results in curvature and slope in the uncorrected absorption spectrum, and this effect will be nearly symmetric between up and down scans. By adding an offset to minimize the effect, backgrounds that are hundreds of times larger than the signal can be accurately removed, as long as we are scanning to a zero-absorption baseline.

   More generally the "slope matching" that lets us infer backgrounds will let us ac-couple signals, which can sometimes improve SNR. On the other hand, if we cannot scan completely off absorption peaks (for example, in high pressure applications) then the slope matching approach fails. Zolo is patenting a new way to remove background that exploits the difference between the up-scan and down-scan due to laser wavelength hysteresis, or the wavelength-scan time delay.
2. Wavelength-scan time delay: Depending on the scanning waveform shape and and laser thermal time constants, the wavelength-modulation waveform (nominally a triangle wave) will be offset relative to the amplitude-modulation waveform by as much as several microseconds. In comparing up and down absorption scans, there is greater symmetry when referencing to the wavelength modulation waveform than to the AM waveform. This is important when taking advantage of the symmetries noted here.
3. The ratio of a near-triangle waveform to a time-shifted copy of itself is (for small shifts) the derivative of a triangle waveform, or a square wave. Hence the flight time delay is properly nulled when there is no square-wave component left in the absorption spectrum, i.e. the up and down scans' average levels are equal. A time delay between S and R of just tens of nanoseconds (several meters of fiber) is easily visible in the Zolo sensor's absorption spectra.
4. True wavelength dependences (modal and etalon noise, actual absorption and passband curvature) should all be symmetric between up and down scans. A seriously asymmetric up/down absorption spectrum implies (1) we are close to the level of random noise; (2) the laser is mode-hopping (laser heating vs cooling will break the up/down symmetry); (3) the laser wavelength is not adjusted properly to be a triangle waveform; or (4) the wavelength-scan time delay noted above is not properly accounted.
   The up/down symmetry is thus a powerful check of time delays, laser health and wavelength scale correction before any baseline correction need be performed. If symmetry is present down to the level of random noise, then both up and down scans should be equally valid. If the symmetry is lost, something is wrong and needs to be fixed.
5. Detector saturation acts like a subtle combination of background offset and flight time delay, and (in contrast to simple backgrounds, flight delays and wavelength scale nonlinearities) is not easily correctable with post-processing. Saturation has to be avoided at the hardware stage. The up/down symmetry will be broken if detector saturation is present.
6. Our detectors have slightly different bandwidths in different gain stages. When the bandwidth of the signal differs from that of the reference then the log-ratio is distorted. The effect looks largely like a flight delay.

Table A-1 lists the measurement errors of concern to us. Some are artifacts that can be corrected during data processing while others such as random noise sources set the fundamental limits to TDLAS sensitivity. Figure A-1 shows examples of spectra contaminated by various artifacts.

noise taxonomy: 1392.8nm, 11 cm air path
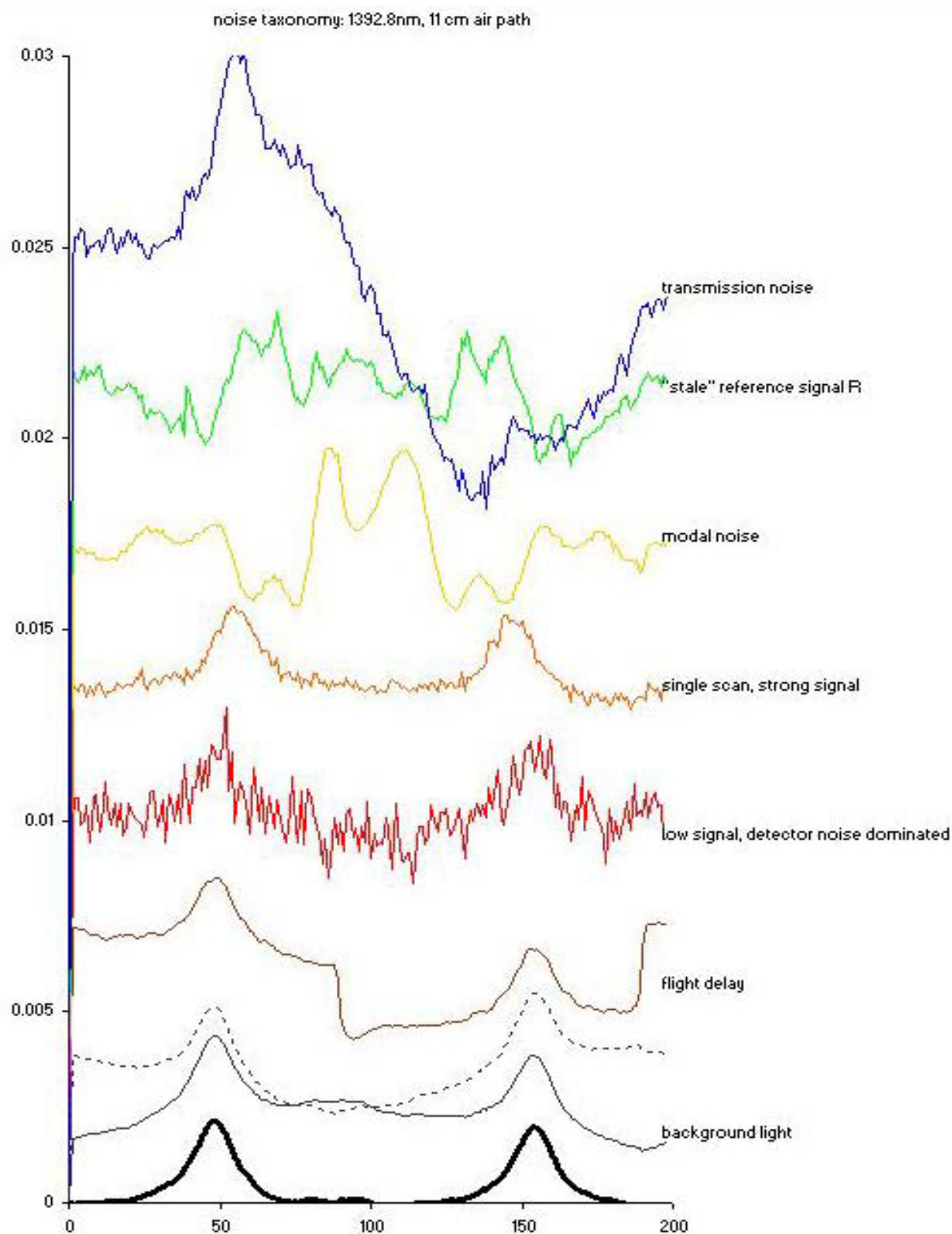
TABLE A-1: TDLAS MEASUREMENT ERROR CONTRIBUTIONS

class	effect	comment	symmetry	systematic?	mitigation
0	shot noise	ultimate limiting noise	0	n	increase detected light
0	detector noise	random, quasi-white noise	0	n	column averaging; limit detector bandwidth
0	fast transmission noise	due to turbulence, typically 1/f	0	n	column averaging; fast scanning
0	slow transmission noise	due to vibrations, large-scale perturbations	0	n	weighted column averaging
0	modal noise	fiber mode dispersion plus mode-dependent los	+	y	reduce mode-dependent loss, fiber length
0	random electronic pickup noise	not synched to scan, will look random usually	0	n	column averaging
0	electronic cross-talk	synchronous with scan	+	y	careful electronic design; system calibration
0	laser noise	usually due to drive current noise	0	n	low-noise drive electronics; live reference
0	quantization error	unlikely except for excessively quiet situations	0	y	AC coupling; added noise
0	detector saturation	will affect waveform shape and bandwidth	+/-	y	reduce signal strength
0	detector bandwidth mismatch	can look light a flight delay error	-	y	equalize bandwidths, slew rates across gains
1	background light	and detector offset	+	y	bandpass filter or remove during processing
1	optically thick absorption	can lead to inaccurate absorption calculation	+	y	carefully account for backgrounds, offsets
1	time error	relative shift, power vs wavelength		y	account during conversion to wavelength
1	flight delay	signal is time-shifted relative to reference	-	y	equalize path delays (optical and electronic)
1	low sampling rate	reduced wavelength resolution	0	y	reduce scan speed or increase sampling rate
1	wavelength scale error	scale and linearity		y	calibrate wavelength scale
2	narrow interfering lines	unwanted absorption peaks	+	y	account for all absorption lines in scan range
2	broad interfering lines	appear as absorption baseline curvature	+	y	removed in quadratic baseline fit
3	path-average approximation	temperature and/or concentration nonuniformity	+	y	model nonuniform-path absorption spectrum
3	external path absorption	molecular absorption outside region of interest	+	y	minimize and/or purge outside path; line choice
3	path length error			y	independent measurement/calibration
3	pressure error			y	independent measurement/calibration
3	line strength error			y	independent measurement/calibration
3	lower-state energy error			y	independent measurement/calibration

class 0: non-correctable effects
class 1: corrected/compensated at pre-processing stage to derive absorption vs wavelength
class 2: corrected at line-fit and integration stage to derive integrated absorption
class 3: corrected at temperature/concentration calculation

APPENDIX B
SPECIFICATION, Zolo Embedded Flight Sensor, HIFiRE Flight 2   **revised:**   **7/15/2009**
                                                                      printed: **9/28/2009**

system overview

The HiFire Flight 2 system demonstrates water absorption spectroscopy for combustion monitoring in a sounding-rocket scramjet.

specification	value	units	measured?
system function/performance			
number of paths	4		by design
wavelength	1396.35 - 1396.65	nm	yes
nominal sensing conditions	scramjet combustor, 10-20% H_2O, T = 1000-2500 K		by design
update rate	5.8	Hz	by design
reported data	detected light by path, column-averaged		by design
measurement details			
static pressure	1 to 2	atm	
temperature	1000-2500	K	
species concentrations	10-20 H_2O, 10-20 CO_2, traces of unburned HCs	%	by design
peak absorbance	10 nominal, 0.1 minimum detectable	%	
absorption width	<10	GHz	
precision/accuracy, T	30/100	K	via post-processing
precision/accuracy, [H2O]	0.5/1.0	%	via post-processing
detected photocurrent range	0.01-200	uA	
intermittency factor	TBD	= transmission SD / AVG	
transmission noise at 10 kHz	<1e-5	fractional, rms/rt-Hz	
optical details			
internal path	100	mm	
external path	<10	mm	
send fiber	SMF-28 in 3 mm monocoil armor, 44 mm bend radius, 1.0 m		
receive fiber	200um/NA0.21 in 3 mm monocoil armor, 44 mm bend radius, 1.0 m		
send spot size	0.35	mm, 1/e2 radius	
receive spot size	1.2	mm, 1/e2 radius	
optical material	fused silica		
polarization sensitivity	TBD		
service temperature, optics	<400 sustained, <550 peak (<10 sec)	degrees C	
environment (electronics)			
operating temperature	0 to 61	deg C	tested
storage temperature	-20 to 85	deg C	tested
humidity range	0 to 99	%	by design
vibration	<15 g, 5 - 2000 Hz	g	tested
shock	60 (30 s duration)	g	by design
air pressure	0-1.2	atm	tested
vacuum compatibility	will survive vacuum (no arcing), may outgas		tested
sealing/ water resistance	not sealed/ not water resistant		
environment (probes)			
operating temperature	-20 to 400	deg C	by design
storage temperature	-20 to 400	deg C	by design
humidity range	0 to 99	%	by design
vibration	<15 g, 5 - 2000 Hz	g	by design
shock	60 (30 s duration)	g	by design
air pressure	0-1.2	atm	by design
vacuum compatibility	will survive vacuum, may outgas		
sealing/ water resistance	not sealed/ not water resistant		
mechanical			
outline and mounting	per Zolo document ZD2000		
control unit dimensions	120 W x 200 D x 60 H	mm^3	by design

optic dimensions	12.7 diameter by 30 long	mm	by design
control unit mass	2.5	kg	by design
optic mass	<0.02	kg	by design

general

input power	24-32	Vdc	
power dissipation	<13 (12 typical)	W	
safety certification	contains Class IIIb source: up to 20 mW total power		
lifetime	1	yr	by design
warranty	1	yr	
documentation	user manual, data sheet		
warm-up time	<15	min	
heat sinking	not required; 1.6 hour self-heat time		

analog outputs

single-end/differential	differential		by design
impedance	50	ohms	by design
voltage range	+/-2.2	V	by design
bandwidth	4.5 nominal	MHz	by design

The stated output voltage range is differentially-driving a high-impedance load. The range is one-half this value when driving 50 ohms.

computer interface

interface to host computer	RS485 on custom HD15		by design
baud rate	115200 (simplex, polling)	bps	by design
serial settings	8 data bits, 1 start bit, 1 stop bit, no parity bit or handshaking		

system connector pinouts (HD15, male)

1	TX-	9	P3+
2	TX+	10	P3-
3	28 Vdc	11	P1+
4	GND	12	P1-
5	28 Vdc return	13	P2-
6	RX-	14	P4+
7	RX+	15	P4-
8	P2+		

data packet

total packet size	1644	bytes	by design
update rate	7 (max)	Hz	by design
format	LSB to MSB (first low bit is start bit)		

packet contents

data	number bytes	value	
packet size	2	bytes	
header	3	bytes	
time since turn-on	4	bytes	
error code array (last 10 errors)	10	bytes	
analog PC board temperature	2	bytes	
+5 Vdc	2	bytes	
-5 Vdc	2	bytes	
LD on/off	1	bytes	
LD voltage	2	bytes	
LD current	2	bytes	
monitor PD current	2	bytes	
LD temperature	2	bytes	
LD TEC error	2	bytes	
LD current setpoint	2	bytes	
LD temperature set point	2	bytes	
path gains	2	bytes	
path 1 column-averaged photo	400	bytes	200 pts, 2 bytes ea
path 2 column-averaged photo	400	bytes	200 pts, 2 bytes ea

path 3 column-averaged photo	400	bytes	200 pts, 2 bytes ea
path 4 column-averaged photo	400	bytes	200 pts, 2 bytes ea
checksum	2	bytes	

detector gain table

gain code	Rf (ohms)
(none)	20 K
A0	60 K
A1	200 K
A0, A1	600 K
TIA	1 M
TIA, A0	3 M
TIA, A1	10 M
TIA, A0, A1	30 M

APPENDIX C: INPUTS TO MEASUREMENT PERFORMANCE MODEL

parameter	symbol	value	units
Boltzmann const	kB	1.38E-23	J/K
speed of light		3.00E+08	m/s
electron charge	e	1.60E-19	C
Avogadro number	N	6.02E+23	
c2	c2	1.438	cm-1/K
mol wt	amu	18	g/mol
molecule mass	m	2.99E-26	kg
pressure	P	1	atm
pathlength (1-pass)	L	5	cm
conc	x	0.13	mol frac
temperature	T	2000	K
ref temperature	T0	296	K
atten coeff	a	0.02	cm-1
1/f noise	nm0	5.00E-04	Hz-1/2
ref frequency	f0	1.00E+04	Hz
1/f noise	nm	1.00E-04	Hz-1/2
c wavelength	wlc	1392.515	nm
c strength	S0c	0.113	cm-2/atm
c lower energy	E"c	590	cm-1
c broadening (self)	gcself	0.49	cm-1/atm
c broadening (air)	gcair	0.1	cm-1/atm
c tempco	nc	0.65	
h wavelength	wlh	1392.806	nm
h strength	S0h	5.50E-03	cm-2/atm
h lower energy	E"h	1227	cm-1
h broadening	ghself	2.70E-01	cm-1/atm
h broadening (air)	ghair	4.52E-02	cm-1/atm
h tempco	nh	6.50E-01	
random velocity	vd	1.92E+03	m/s
doppler width	nud	1.38E+09	Hz
doppler width	nudcm	4.60E-02	cm-1
doppler FWHM	dnd	5.42E-02	cm-1
part fcn a	a	-94.3	
part fcn b	b	0.819	
part fcn c	c	7.40E-05	
part fcn d	d	4.24E-07	
std part fcn	QT0	1.66E+02	(values for mid-ra
part fcn	QT	5.23E+03	
c collisional width	gcc	8.36E-02	cm-1
h collisional width	gch	4.14E-02	cm-1
c total FWHM	gc	1.11E-01	cm-1
h total FWHM	gh	7.97E-02	cm-1
c strength	STc	6.09E-03	cm-2/atm
h strength	STh	4.14E-03	cm-2/atm
c pk abs	apkc	7.10E-02	

parameter	symbol	value	units
probe			
probe aperture	wc	3.56	mm
send focal length	fp	10	mm
send NA	Nap	0.11	
send core	ap	0.0045	mm
receive focal length	fc	16.95	mm
receive NA	Nac	0.21	
receive core	ac	0.1	mm
length tolerance	dL	1	cm
incidence angle	qinc	0	radians
angle tolerance	dqinc	0.01	radians
scatter spread	dqscatt	0.1	radians
fill factor	k	0.67	
surface reflectivity	Rsurf	0.5	
target spot radius	ws	0.29	mm
light collection efficien	eta	1.7E-01	
electro-optic package			
laser power	PL	0.001	W
detector responsivity	Rdet	0.9	A/W
internal efficiency	hint	0.01	
detector noise	nd0	1.00E-12	A/Hz1/2
ref frequency	f0	1.00E+04	Hz
detector noise	ndet	5.00E-12	A/Hz1/2
detector bandwidth	BW	2.4E+06	Hz
scan range	D	2.3E+00	cm-1
background light	Ibk	1.00E-09	A
scan frequency	fscan	5.0E+04	Hz
detected photocurrent	Idet	1.3E-06	A
derived spectrum			
total noise density	nTOT	2.E-11	A/Hz1/2
artifact level	aart	5.0E-04	
measurement time	t	0.08192	s
useful fraction	fcomp	0.7	
c spectral fraction	fspecc	0.049	
h spectral fraction	fspech	0.035	
effective time	teffc	0.0028	s
effective time	teffh	0.0020	s
absorption uncertainty	amin	0.00034	
alt uncertainty	amin2	0.00050	
measurement result			
temperature error	dT	46.9	degK